

# Lawrence Berkeley National Laboratory

## Recent Work

### Title

Aerosol Fragmentation Driven by Coupling of Acid-Base and Free-Radical Chemistry in the Heterogeneous Oxidation of Aqueous Citric Acid by OH Radicals.

### Permalink

<https://escholarship.org/uc/item/2hx5q6wq>

### Journal

The journal of physical chemistry. A, 121(31)

### ISSN

1089-5639

### Authors

Liu, Matthew J  
Wiegel, Aaron A  
Wilson, Kevin R  
[et al.](#)

### Publication Date

2017-08-01

### DOI

10.1021/acs.jpca.7b04892

Peer reviewed

1 **Aerosol Fragmentation Driven by Coupling of Acid-Base and Free Radical**  
2 **Chemistry in the Heterogeneous Oxidation of Aqueous Citric Acid by OH**  
3 **Radicals**

4 Matthew J. Liu,<sup>a,b</sup> Aaron A. Wiegel,<sup>a</sup> Kevin R. Wilson,<sup>†a</sup> and Frances A. Houle<sup>†a</sup>

5 <sup>a</sup>Lawrence Berkeley National Laboratory, Chemical Sciences Division, Berkeley, CA, USA  
6 94702

7 <sup>b</sup>University of California, Berkeley, Department of Chemical and Biomolecular Engineering,  
8 Berkeley, CA, USA 94720

9<sup>†</sup> Authors to whom correspondence should be addressed:

10 Frances A. Houle ([fahoule@lbl.gov](mailto:fahoule@lbl.gov)) and Kevin R. Wilson ([krwilson@lbl.gov](mailto:krwilson@lbl.gov))

11

12 **Abstract**

13 A key uncertainty in the heterogeneous oxidation of carboxylic acids by hydroxyl radicals (OH)  
14 in aqueous phase aerosol is how the free radical reaction pathways might be altered by acid-base  
15 chemistry. In particular, if acid-base reactions occur concurrently with acyloxy radical formation  
16 and unimolecular decomposition of alkoxy radicals, there is a possibility that differences in  
17 reaction pathways impact the partitioning of organic carbon between the gas and aqueous phases.  
18 To examine these questions, a kinetic model is developed for the OH initiated oxidation of citric  
19 acid aerosol at high relative humidity. The reaction scheme, containing both free radical and  
20 acid-base elementary reaction steps with physically validated rate coefficients, accurately  
21 predicts the experimentally observed molecular composition, particle size, and average elemental  
22 composition of the aerosol upon oxidation. The difference between the two reaction channels  
23 centers on the reactivity of carboxylic acid groups. Free radical reactions mainly add functional  
24 groups to the carbon skeleton of neutral citric acid, because carboxylic acid moieties deactivate  
25 the unimolecular fragmentation of alkoxy radicals. In contrast, the conjugate carboxylate groups  
26 originating from acid-base equilibria activate both acyloxy radical formation and carbon-carbon  
27 bond scission of alkoxy radicals, leading to the formation of low molecular weight, highly  
28 oxidized products such as oxalic and mesoxalic acid. Subsequent hydration of carbonyl groups in  
29 the oxidized products increases the aerosol hygroscopicity and accelerates the substantial water  
30 uptake and volume growth that accompany oxidation. These results frame the oxidative lifecycle  
31 of atmospheric aerosol: it is governed by feedbacks between reactions that first increase the  
32 particle oxidation state, then eventually promote water uptake and acid-base chemistry. When  
33 coupled to free radical reactions, acid-base channels lead to formation of low molecular weight  
34 gas phase reaction products and decreasing particle size.

35

36

37

38

39

40 **I. Introduction**

1

2

1

41Sub-micron-sized atmospheric organic aerosols profoundly influence Earth's climate by  
42interacting with incoming solar radiation and serving as cloud condensation nuclei, altering  
43cloud formation and albedo.<sup>1</sup> The extent to which these processes occur is determined by the  
44size, chemical composition, shape, and lifetime of the aerosol, making their characterization  
45crucial for the predictive accuracy of air quality and climate models. However, describing the  
46oxidative evolution (aging) of organic aerosol is difficult due to the extensive and complex  
47chemical reactions that occur. The oxidation of organic aerosol is thought to have a major  
48influence on particle composition and size, leading to numerous studies of the heterogeneous  
49oxidation of organic particles by gas-phase hydroxyl radicals (OH). Laboratory investigations of  
50model atmospheric aerosols<sup>2</sup> provide insight into how the formation of new oxygenated  
51functional groups (i.e. functionalization) and C-C bond scission (i.e. fragmentation) reactions  
52together alter particle composition and size.<sup>3-7</sup> These experimental studies are particularly  
53valuable when coupled with detailed kinetics models since the resulting predictive description  
54connects key elementary reaction steps to changes in the physical properties of the aerosol.

55

56When an organic aerosol becomes very heavily oxidized, significant concentrations of carboxylic  
57acid groups build up on the particle surface.<sup>8</sup> As a result, initially hydrophobic aerosol develops  
58hydrophilic character. Under humid conditions, water will accumulate on a hydrophilic surface  
59over time, transforming the reaction environment from a purely organic matrix into an aqueous  
60solution. This is a very late phase of chemical ageing of a chemical reduced aerosol, and gaining  
61an understanding of the factors that control reactivity in this regime and what role may be played  
62by carboxylic acid moieties are the primary goals of this work.

63

64 There have been a number of important studies of the aqueous phase chemistry of oxidized  
65 aerosol constituents that examine reaction rates and mechanisms<sup>9-15</sup> as well as the relationship  
66 between aerosol phase state, heterogeneous reaction rate and ultimately cloud nucleation  
67 activity.<sup>16-25</sup> In general these systems exhibit substantial C-C bond fragmentation and  
68 volatilization, in contrast to what is generally observed in the heterogeneous oxidation of reduced  
69 organics.<sup>20, 26</sup> For example, levoglucosan, an anhydrosugar, has been widely studied as a model  
70 for aqueous biomass derived aerosol, undergoes significant fragmentation.<sup>21-22, 27-29</sup> The same  
71 behavior is reported for the heterogeneous oxidation of aqueous erythritol, another highly  
72 oxygenated model system.<sup>20, 30</sup> In this case, Kessler et. al.<sup>20</sup> found evidence that hydrogen  
73 abstraction by OH from a hydroxyl group leads to  $\alpha$ -hydroxy alkoxy radical formation and  
74 subsequent decomposition by C-C bond scission.

75

76 The differences in reactivity between heavily and lightly oxidized systems originate from the  
77 presence of oxygen-containing functional groups located on or adjacent to peroxy and alkoxy  
78 radical intermediates, whose chemistry in turn controls the extent of fragmentation and  
79 subsequent volatilization.<sup>20, 31</sup> For example, for a series of structurally related model dicarboxylic  
80 acid aerosol with a common C<sub>4</sub> backbone, the distribution of primary, secondary and tertiary  
81 peroxy and alkoxy radicals, formed after the initial OH radical reaction, was observed to play a  
82 large role in ultimately governing the quantity and identity of smaller molecular weight C-C  
83 bond scission products.<sup>16-18</sup> In most of these previous studies experimental observations were  
84 rationalized solely by free radical reaction pathways initiated by OH. However, we expect that  
85 for the vast majority of highly oxidized ambient organic aerosol (e.g. secondary organic aerosol),  
86 which are hydrophilic in nature, the presence of an aqueous phase will lead to carboxylic acids

87being in equilibrium with their conjugate base. Thus, OH will react with both neutral and ionic  
88forms. Acid-base chemistry should occur simultaneously with free radical oxidation, and  
89constitute an important aging mechanism for particles in the troposphere.

90

91To our knowledge there have been only a few detailed experimental investigations<sup>32-36</sup> of  
92heterogeneous OH reactions in systems where free radical and acid-base chemistry can occur  
93simultaneously. In this work, we investigate the heterogeneous OH oxidation of aqueous citric  
94acid (CA) aerosol by OH. CA is a reasonable model for highly oxidized organic aerosol  
95(C<sub>6</sub>H<sub>8</sub>O<sub>7</sub>), containing three carboxylic acid functional groups and a single alcohol moiety. CA  
96should exhibit many of the OH-driven aging pathways that occur in secondary organic aerosol.  
97Because of its low pKa, CA is expected to react with OH in both neutral and acid-base forms.  
98We develop a molecular level kinetic description of the chemistry for this system using the  
99generalized oxidation mechanism for triacontane as a foundation.<sup>8</sup> The model predictions are  
100compared to an extensive experimental dataset obtained previously by Davies and Wilson,<sup>37</sup>  
101which includes the CA decay kinetics, product mass spectra, elemental ratios, and aerosol size;  
102all of which evolve with OH exposure. We focus on the dataset obtained at a relative humidity  
103(RH) of 64.5%, where the aerosol is liquid and well-mixed on the timescale of the OH reaction  
104frequency. Since the aerosol is an aqueous solution of CA in equilibrium with its conjugate base,  
105we have included reactions of OH with ionic species as well as with neutrals. We have performed  
106simulations for three scenarios to elucidate how key reaction steps control reactivity and physical  
107properties of the aerosol in aqueous vs. non-aqueous aerosol systems. We find that only those  
108simulations that include both acid-base and free radical pathways yield model predictions  
109consistent with the global experimental dataset.

110

### 111II. Model Framework

112Complex sets of chemical reactions are traditionally analyzed using sets of coupled ordinary  
113differential equations in which continuous variables evolve deterministically. Although this  
114reasonably describes test-tube sized or larger systems,<sup>38</sup> as system size decreases to the size of an  
115aerosol, discreteness and stochasticity can have much greater impacts on system behavior. Under  
116such conditions, molecular populations are better viewed as integer variables evolving  
117stochastically. Kinetiscope<sup>39</sup>, the software used here, is based on a stochastic algorithm that  
118propagates a simulation by randomly selecting among probability-weighted elementary reaction  
119steps (events).<sup>40-41</sup> The rate law for each of elementary step is used to calculate the probabilities,  
120and establish an absolute time base for direct comparison of simulations to experiment. The  
121method has been shown to be a rigorous solution to the master equation for Markov processes. It  
122has been extended to simulate kinetics in systems with variable volume<sup>42</sup> and is well suited to  
123cases such as aqueous citric acid aerosol oxidation. Additional information is available on the  
124software's website and in prior work on aerosol oxidation.<sup>31, 43</sup> Reaction mechanisms are  
125constructed inductively, that is, by starting from the simplest description and adding new reaction  
126steps when the simulation results fail to agree with experiment. Rate coefficients for each step  
127are taken directly from literature, calculated from experimental data or quantum theory, or  
128estimated using quantitative structure-activity relationship models. Initial concentrations are used  
129to replicate experimental conditions. Further discussion of the methodology is presented in the  
130Supplementary Information (SI), section S1.

131

132The current model includes a number of elements previously developed<sup>8, 31, 43</sup> to describe the  
133multiphase chemistry of organic aerosols. These elements (outlined briefly in Sec. IIa), include  
134the simulation geometry, kinetic descriptions of OH sticking and reaction, evaporation of  
135products as well as the central pathways for peroxy and alkoxy reactions. Several new elements,  
136outlined in detail in Sec. IIb-d, have been added to simulate the heterogeneous reaction of CA  
137aerosol by OH. They include acid-base reactions and equilibria, and accurately capture the  
138changes in aerosol size during oxidation due to dynamic uptake and release of ambient water.

139

#### 140a. *OH uptake and reaction, evaporation, and radical reaction pathways*

141*OH uptake.* As described in previous studies, the reaction rate of OH at the surface of the aerosol  
142is controlled by two separate elementary steps.<sup>8, 31, 43</sup> First the OH absorbs to a surface site from  
143the gas phase, then it reacts with CA or its products. The absorption step is described by a  
144pseudo first order rate coefficient ( $k_{ad}$  in Table 1).  $k_{ad}$  depends on three factors: the OH  
145concentration in the gas phase, the gas-surface collision frequency, and the OH sticking  
146probability. While two of these are known quantities, the sticking probability is usually not  
147known and for this system is expected to be rather complex since the aerosol surface has  
148substantial water coverage in addition to organic reactants and products.<sup>37</sup> Accordingly, a value  
149of  $0.052 \text{ s}^{-1}$  is determined for  $k_{ad}$  by adjusting it until the calculated citric acid concentration vs  
150time curve is in quantitative agreement with experiment.<sup>8, 43</sup> The collision frequency of OH,  $k_{coll}$ ,  
151at a density of  $7.5 \times 10^{10} \text{ molec/cm}^3$  with the  $10^{-14} \text{ cm}^2$  surface area of the reaction compartment  
152(Section II d) is calculated to be  $12.4 \text{ s}^{-1}$ . Since  $k_{ads} = \alpha k_{coll}$ , this gives a value of  $4.2 \times 10^{-3}$  for  $\alpha$ ,  
153the sticking coefficient. This is in the range estimated for  $\alpha$  in simulations of OH reacting with  
154squalane ( $10^{-4}$ )<sup>43</sup> and triacontane ( $5 \times 10^{-5}$ , calculated from the reported rate coefficient).<sup>8</sup> Since

155the sticking coefficient for water to water surfaces is 1,<sup>44</sup> and OH to water is in the same range,<sup>45</sup>  
156the low value suggests that the outer surface of the aerosol has a strongly organic character  
157despite the significant amount of water present. All other coefficients in the mechanism are  
158derived from experiment and theory.

159

160*Evaporation.* The simulated aerosol volume dynamically evolves both by the formation of higher  
161density reaction products that bind water formed by OH reactions or accrete waters of solvation  
162from the ambient, and by the evaporation of high volatility small molecule products and  
163eventually their water shells. Loss of water is assumed to be instantaneous following desorption  
164of products from the aerosol surface. Products containing 2 carbons, such as oxalic acid, have  
165much higher vapor pressure than those with 3 carbons and greater,<sup>46</sup> and are assumed to be the  
166only ones that undergo significant evaporation. Their vapor pressures are set to be  $1 \times 10^{-4}$  Pa, a  
167value typical for small dicarboxylic acids at room temperature.<sup>46</sup> The evaporation rate coefficient  
168computed from this vapor pressure and the simulation geometry, as described in Wiegel et al,<sup>8, 31</sup>  
169is  $0.35 \text{ s}^{-1}$ .

170

171*Radical reaction pathways.* Because the possible reactions are relatively few, the elementary  
172steps used to describe the heterogeneous reaction of CA with OH are written explicitly (i.e.  
173involving individual molecules) rather than using the lumped reaction scheme based on  
174functional group chemistry introduced previously to model the multi-generational oxidation of  
175alkanes.<sup>8, 31</sup> As shown in Table S1 in the SI, the full range of possible reaction products is  
176considered and includes C<sub>6</sub> functionalization products as well as C<sub>2</sub>-C<sub>5</sub> species formed via C-C



177bond scission reactions. These product species are formed via the generic elementary reaction  
178steps, shown in Figure 1, that have been used in previous studies.<sup>4-5, 8, 31, 43, 47-48</sup>

179

180Briefly, OH can abstract a hydrogen atom from a  $-CH_2$  or  $-OH$  moiety located on CA or its  
181reaction products (generically represented as RH in Figure 1). The rate coefficient for H-  
182abstraction from these sites are taken from the literature and shown in Table 1. The resulting H-  
183abstraction reaction at the  $-CH_2$  group produces an alkyl radical (R), which is rapidly converted  
184(in the presence of  $O_2$ ) into a peroxy radical ( $RO_2$ ).  $RO_2$  is the central intermediate that controls  
185much of the oxidative transformation of CA and its subsequent products. For instance,  $RO_2 +$   
186 $RO_2$  reactions produce either stable products with new alcohol and carbonyl functionalities or  
187alkoxy radicals (RO). Previous work<sup>31</sup> has shown that the aerosol oxidation chemistry is  
188consistent with 90% of the secondary  $RO_2 + RO_2$  reactions yielding stable products (i.e. carbonyl  
189and alcohol), and the remaining 10% forming alkoxy radicals and  $O_2$ . H abstraction from the  $-$   
190OH group directly forms an alkoxy (RO) radical or, in the case of an  $-OH$  group on a carboxylic  
191acid, an acyloxy radical. Unimolecular decomposition of alkoxy and acyloxy radicals as well as  
192intermolecular H-abstraction by RO are included in the model. As shown in Figure 1,  
193hydroperoxide ( $ROOH$ ) products are formed by the  $RO_2 + HO_2$  reaction.

194

195In following sections, we describe extensions to the oxidation mechanism. They include the  
196implementation of the new acid-base reaction steps, the calculation of their rate constants, and a  
197description of how these acid-base equilibria are coupled to the free radical reaction scheme  
198described above. This is followed by a description of how water is included in the simulation to  
199order to properly account for the hygroscopic growth of the aerosol during oxidation.

200

### 201**b. Acid-Base chemistry**

202The aqueous environment requires the inclusion of acid-base chemistry in modeling the  
203oxidative evolution of the aerosol. While free radical chemistry in hydrophobic organic aerosol is  
204well-constrained by known reaction pathways and rate coefficients, little work has explicitly  
205focused on how free radical chemistry is modified in aqueous organic aerosol where acid-base  
206chemistry occurs simultaneously. CA has a  $pK_{a1}$  of 3.13, and dissociates in water to produce  
207hydronium and citrate, the conjugate base of CA. This relatively acidic environment leads to  
208further deprotonation of the numerous triacid and diacid products (see Table S1) formed from  
209CA oxidation. Thus, we expect the formation of radical anions as the system is oxidized, and are  
210interested in how the reactivity of these radical anions differs from their neutral counterparts (e.g.  
211citrate vs citric acid). In particular, we focus on the unimolecular fragmentation rates of anionic  
212alkoxy radicals compared to their neutral analogs. Because several key rate coefficients have not  
213been measured, we used *ab initio* calculations of the reaction barriers to estimate them.

214

215Using Gaussian09,<sup>49</sup> the ground state energy of the radical is obtained by optimization of all its  
216conformers using the SMD/IEF-PCM solvent model for water and the M06-2x functional and the  
2176-31G(d,p) basis set. The solvent model was shown by Marenich et. al.<sup>50</sup> to reduce mean  
218unsigned errors in the solvation energies of both neutral and charged species while the functional  
219was shown by Walker et. al.<sup>51</sup> to be a superior choice compared to B3LYP in systems with  
220dispersion and ionic hydrogen-bonding interactions. Vibrational frequencies of the ground state  
221are computed at the same level of theory to ensure the optimized structure corresponds to a local  
222minimum. For the transition state calculation, the Berny option with a calculation of force  
223constants is used. The length of the fragmenting C-C bond is set to the value obtained by a

224relaxed potential energy surface scan for a local maximum in total molecular energy. The barrier  
 225height for dissociation,  $E_b$ , is taken as the difference between the ground and transition state  
 226energies. Rate coefficients for  $\beta$  C-C bond scission of substituted alkoxy radicals are estimated  
 227using the following structure-activity relationship model developed by Vereecken and Peeters,<sup>52</sup>

$$k_{diss}(T) = L \times A_{TST}(298 K) \times \left(\frac{T}{298 K}\right)^{\ddagger} \quad (\text{Eq. 1})$$

229where  $L$  is the number of identical bond scissions and  $A_{TST}(298 K)$  is the pre-exponential  
 230factor at 298 K based on Transition State Theory. Further details are presented in section S5  
 231of the SI.

232

233As observed in previous work<sup>31, 52-53</sup> and further confirmed by this set of calculations, the barrier  
 234height for  $\beta$ -scission of an alkoxy radical is found to be lowered when a ketone or hydroxyl  
 235functional group is located on an adjacent carbon atom as shown in Scheme 1. The reduction in  
 236barrier height is significant, such that unimolecular decomposition of activated RO is the primary  
 237sink for alkoxy radicals rather than, for example, hydrogen abstraction (i.e. RO + RH).

238

239 As shown in Scheme 1c, the barrier height for the already-activated alkoxy radical is reduced  
 240even further when the adjacent carboxyl group is deprotonated. Indeed,  $\cdot\text{COOH}$  is reported

241to be a fleeting radical while the  $\cdot\overset{-\ddagger}{\text{COO}}^{\ddagger}$  radical anion has been observed to form in aqueous

242 solutions due to stabilization by the solvent.<sup>54-57</sup> However, activation of the carboxylate group is

243 not limited to those pathways that form  $\cdot\overset{-\dot{i}}{COO}^i$ . As shown in Scheme 2, formation of a larger  
244 radical anion is still more favorable than its neutral form. The difference in fragmentation rate  
245 coefficients calculated using these barriers confirms the necessity of including acid-base  
246 chemistry in the model to capture the low energy reaction pathways.

247

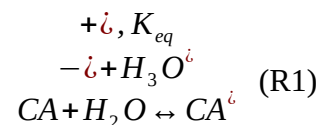
#### 248c. *Inclusion of rapidly maintained equilibria.*

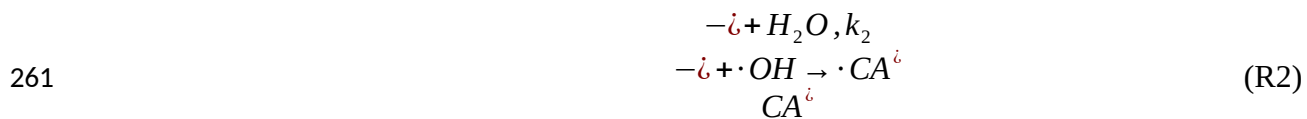
249 Explicit simulations of rapidly maintained acid-base equilibria using stochastic methods are  
250 exceedingly slow.<sup>39, 58-59</sup> This is because reaction steps at equilibrium have a high probability of  
251 being selected relative to the other reaction steps, and the simulation's timescale barely advances.  
252 Thus, explicit inclusion of equilibrium steps for the deprotonation and protonation of carboxyl  
253 groups in CA is impractical, and they are included implicitly, as described below. Extensive  
254 checks were made to verify that this approximation does not change the simulation results; they  
255 are presented in section S3 of the SI.

256

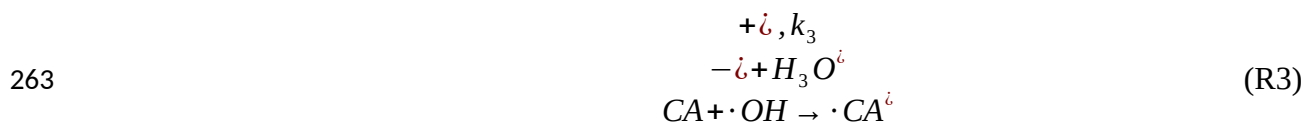
257 The deprotonation of CA to form citrate and its subsequent reaction with OH can be described by  
258 the following steps, where R1 and R2 are added together, and explicit treatment of water and  
259 hydronium formation becomes implicit:

260





262



264 The forward rate of reaction ( R3 )  $\frac{CA}{\dot{i}}$ , where  $\frac{CA}{H}$ . This yields the rate constant

265  $k_3 = K_{eq} k_2 \frac{H}{[H_2O]}$ . In explicit model runs performed to test this approximation,  $\frac{CA}{[CA]}$  has

266a nearly constant ratio (section S3 in the SI). This justifies the assumption that a strict  
 267 equilibrium between water and hydronium is maintained, i.e. pH is constant. By using the

268 average value of  $\frac{H}{3O} \frac{[H_2O]}{[H_2O]}$  from the explicit model,  $k_3$  is easily computed and is shown in

269 Table 1. Thus,  $CA$  is no longer explicitly included in the mechanism, since its concentration  
 270 is embedded in the rate constant  $k_3$  which is proportional to the CA acid-base,  $K_{eq}$ . We extend  
 271 this method of modeling protonation and deprotonation to all other acid products in the system  
 272 by using their respective  $K_a$  values (Table S1 in the SI), making simulation runtimes much more  
 273 practical.

274

275 Some reaction products observed in the experiment contain new carbonyl functionalities. As a  
 276 result, hydration reactions of these species ( $R=O \leftrightarrow R(OH)_2$ ) are included in the simulations. The  
 277 equilibrium constants  $K_h$  for these products, described below, are computed using structure  
 278 activity relationships in Ref<sup>60</sup> and listed in Table S1 in the SI. In the simulation, hydration is  
 279 assumed to be instantaneous for species with  $K_h > 100$ . Otherwise, using the treatment for acid-  
 280 base chemistry described above,  $K_h$  is combined with the OH abstraction reaction coefficient for  
 281 the alcohol form (Table 1) to generate an effective rate coefficient.

282

**283d. Treatment of water and aerosol volume.**

284 As will be discussed further below, the experimentally observed CA aerosol volume increases by  
 285 ~50% during the initial stages of the reaction. In the simulations, the volume is calculated

286dynamically using the instantaneous amounts and densities of all species present (Table S1 in the  
287SI). This allows concentrations and reaction rates to be continuously corrected as the volume  
288changes.

289

290The substantial volume increase is much larger than can be rationalized solely by the formation  
291of oxidation products. Previous studies report a variety of approaches to estimate the  
292hygroscopicity of oxidized aerosol, the simplest of which uses O/C as the primary predictor.<sup>61-62</sup>  
293Suda et. al.<sup>63</sup> examined the influence of the location and number of functional groups on organic  
294aerosol hygroscopicity, and concluded that hydroxylation is a key pathway by which aerosols  
295become more hygroscopic. In view of the literature, the likeliest explanation for the initial  
296increase in volume is uptake of ambient water, promoted by formation of new hygroscopic  
297species during oxidation. After the initial period of growth, the subsequent volume loss  
298originates from the desorption of volatile organic compounds and their waters of solvation when  
299fragmentation becomes kinetically significant.

300

301In the model described here, the rates of adsorption, absorption and desorption of water  
302molecules are assumed to be very fast relative to the chemical reaction rate, and therefore are not  
303treated explicitly. Instead, each species in the simulation is assumed always to have a number of  
304water molecules solvating it, contributing to its effective density. Because few data are available  
305for the size of stable water solvation shells for species involved in the oxidation reactions,  
306estimates are made based on the literature value of 6-7 waters per CA molecule, computed for  
307neutral species from room temperature solubility data.<sup>64</sup> The average number of waters, 6.5, are  
308apportioned among the functionalities as 2 waters per  $-\text{COOH}$  moiety, and 0.5 waters per alcohol

309or carbonyl moiety. If a species can deprotonate to form hydronium, the hydronium is modeled  
310as having 3 additional water molecules.<sup>65</sup> We assume that the formation of two adjacent alcohol  
311groups via the hydration of carbonyls results in the addition of 0.5 waters to the solvation shell.  
312Because the model does not explicitly contain ionic species their waters are included indirectly.  
313The percent CA dissociation obtained from explicit model simulations is used as a weighting  
314factor to calculate the average number of water molecules associated with each acidic species.  
315The total number of waters estimated using these criteria for each species is shown in Table S1 in  
316the SI. The partial volume of water is added to the molar volume of the organic to estimate the  
317density of each organic+water group. These values are also listed in Table S1.

318

319In addition to changes of volume and concentrations in the particle, and thus reaction rates,  
320changes in the surface to volume ratio of the aerosol impact the relative importance of surface  
321and bulk chemical reactions. Because the aqueous aerosol has low viscosity, it is represented  
322using a single instantaneously mixed compartment rather than multiple diffusion-coupled  
323compartments, which has been shown to be valid for reactions in well-mixed aerosol.<sup>31, 43</sup> This is  
324computationally efficient but poses challenges for proper weighting of surface to volume kinetics  
325when there are large volume changes. Bulk reactions occur throughout the volume, but OH  
326adsorption only takes place at the surface. To ensure that this balance is correctly represented in  
327the simulations, the single compartment is treated as a slim 1 nm x 1 nm x  $R/3$  nm cuboid in the  
328aerosol, where the outer surface of the aerosol is represented as a fixed 1 nm<sup>2</sup> square and  $R$  is the  
329instantaneous radius of the spherical aerosol that is being simulated. This is implemented by  
330assuming that the number of surface sites (1 site per initial surface CA molecule within 1 nm of  
331the surface, calculated from the density of CA in solution), available for adsorption and  
332desorption as the reaction proceeds, is constant. Consequently, the dimension of  $R/3$  is equal to



333the ratio of the instantaneous volume to the fixed surface area. This representation maintains the  
 334correct scaling between compartment volume and area of the spherical aerosol modeled in the  
 335experiment, and thus the correct weighting of surface and bulk chemical processes.

336

337***e. Photolysis of hydroperoxides***

338There are reaction pathways in the model that produce hydroperoxides (ROOH). As such we  
 339consider that possibility that if these species are formed that they could be photolyzed by the 254  
 340nm light source used in the experiment to generate OH. We assume that the photon flux incident  
 341on particle phase ROOH is the same as that for ozone in the flow tube reactor (value in Table 1).  
 342The photolysis of ozone can be described as:



344where we determine value of  $k_p$  that best replicates the experimental [OH]. A value of  
 345  $k_p = 0.5 s^{-1}$  produces an average [OH] which matches experiment. From this value, we can  
 346estimate the rate coefficient for ROOH photolysis by scaling  $k_p$  by ratio of ROOH and  $O_3$   
 347cross sections ( $\sigma$ ) at 254 nm and 293.15K,

348

$$k_{photolysis} = \frac{k_p * \sigma_{ROOH}}{\sigma_{ozone}} \quad (R5)$$

349  $\sigma_{ROOH}$  is estimated by averaging values for small hydroperoxides  $CH_3OOH$  and  
 350  $HOCH_2OO$  (see Table 1).<sup>66</sup>

351

### 352III. Results

353The simulation results are compared with previous measurements reported in Davies and  
354Wilson.<sup>37</sup> As detailed below, the experimental measurements include: (a) the reactive decay of  
355CA, (b) average aerosol elemental composition, product mass spectra and formation kinetics, (c)  
356particle volume as a function of OH exposure. A successful model will generate predictions that  
357are within the experimental errors for this entire suite of measurements. Three model scenarios  
358are considered and compared with experiment in order to explore separately the effects of free  
359radical and acid-base chemistry, and to assess the importance of fragment evaporation on the  
360physiochemical evolution of the aerosol. As summarized in Table 2, Scenario 1 includes free  
361radical chemistry only without evaporation; Scenario 2 includes free radical and acid base  
362chemistry without evaporation and Scenario 3, the most complete simulation, includes free  
363radical + acid base chemistry and evaporation of C<sub>2</sub> reaction products.

364

#### 365 a. *Citric Acid Decay as a Function of OH Exposure*

366The normalized decay of CA as a function of OH exposure is plotted for the experiment and the  
367three model scenarios in Figure 2. All three scenarios accurately predict, within experimental  
368error, most of the exponential decay of CA observed in the experiment. The first few  
369experimental points at low exposure are the exception: they deviate from a purely exponential  
370function. The reason for this is unclear, and is not predicted by any of the model scenarios.  
371Phenomenological CA disappearance rate constants ( $k_{obs}$ ) are extracted from exponential fits to  
372the experiment and simulations. As shown in Table 3 the range is relatively small, but Scenario 3  
373is in closest agreement with observations.

374

375 **b. Average Aerosol Elemental Composition and Product Mass Spectra**

376 The average aerosol elemental composition observed during the reaction is shown in Figure 3.  
377 This representation, known as a van Krevelen diagram, shows the relationship between the  
378 hydrogen-to-carbon (H/C) and oxygen-to-carbon (O/C) ratios. Before reaction the elemental  
379 composition of CA is H/C = 1.33 and O/C = 1.16. Both the H/C and O/C change substantially  
380 during the experiment yielding a final average elemental composition of H/C = 1.1 and O/C =  
381 1.4 at  $[\text{OH}]t = 4.4 \times 10^{12} \text{ molec. cm}^{-3} \text{ s}$ . All three scenarios predict similar van Krevelen trends  
382 and all are within the overall experimental error of the experiment.

383

384 Despite similarities in average aerosol composition, significant differences among the scenario  
385 predictions appear when they are compared to the experimentally observed population of major  
386 reaction products detected via aerosol mass spectrometry.<sup>37</sup> The ionization source used in the  
387 experiments is Direct Analysis in Real Time (DART), which produces negatively charged M-H<sup>-</sup>  
388 ions. For example, neutral CA ( $\text{C}_6\text{H}_8\text{O}_7$ ) molecules appear in the negative ion mass spectrum at  
389  $m/z = 191.02$  ( $\text{C}_6\text{H}_7\text{O}_7^-$ ). The experimental data are not corrected for ionization cross section  
390 differences. Data are shown in Figures 4 and 5.

391

392 It is clear from Figure 4 that only Scenario 3 predicts all 5 major products observed aerosol mass  
393 spectra. There is also good agreement between Scenario 3 and the experimental mass spectrum  
394 recorded at lower OH exposures ( $\text{OH exposure} = 2.2 \times 10^{12} \text{ molec. cm}^{-3} \text{ s}$ ) as shown in Figure S5  
395 in the SI, indicating that this scenario replicates all of the major reaction products observed over  
396 the course of the reaction. Scenarios 1 and 2 fail to capture the dominant product peak observed  
397 at  $m/z = 116.98$ , which is assigned to mesoxalic acid. Furthermore, Scenario 2 predicts little if

398any  $m/z = 207.01$ , assigned to the  $C_6H_8O_8$  functionalization product (i.e. CA + an alcohol group).  
399Scenario 1 produces only small quantities of the product at  $m/z = 133.01$ , assigned to the  $C_4$   
400fragmentation product malic acid ( $C_4H_6O_5$ ).

401

402The experimental mesoxalic acid ( $m/z = 116.98$ ) formation kinetics are compared to predictions  
403by the model scenarios in Figure 6. It is clear that while all the scenarios produce some  
404mesoxalic acid, since there are multiple pathways for its formation, Scenarios 1 and 2 produce  
405mesoxalic acid either too quickly or slowly relative to the experiment. Only Scenario 3 correctly  
406predicts the experimentally observed mesoxalic acid formation as a function of OH exposure.

407

#### 408c. *Aerosol volume*

409The measured change in aerosol volume vs. OH exposure is shown in Figure 7. At the start of  
410oxidation the aerosol grows by ~50% from the initial unreacted aerosol. As noted above, the  
411magnitude of this volume increase cannot be explained solely from a change in density as CA is  
412consumed and the reaction products observed in the experimental mass spectrum form (Figure  
4134). Rather it is more likely that much of the observed growth is due to an increase in the aerosol  
414hygroscopicity (water uptake). The measured aerosol volume reaches a maximum around an OH  
415exposure of  $\sim 2 \times 10^{12}$  molec.  $cm^{-3}$  s after which it decreases towards the end of the reaction, with  
416a final volume ~25% larger than the unreacted CA aerosol. It is clear from the experiment that  
417there is a complex interplay between the formation and evaporation of reaction products and  
418water uptake.

419

420Figure 7 compares experiment with predictions from Scenario 1 (radical only chemistry, no  
421evaporation) and Scenario 2 (radical + acid-base chemistry, no evaporation) and Scenario 3  
422(radical + acid-base chemistry, with evaporation). Scenario 1 under-predicts the magnitude of  
423the change in aerosol volume with OH exposure, while Scenario 2 greatly overestimates the  
424change in aerosol volume. Neither Scenario 1 or 2 includes product evaporation, and thus as  
425expected cannot capture the decrease in volume at larger OH exposures. In contrast, Scenario 3  
426produces the correct shape, within experimental uncertainty, as well as the absolute magnitude of  
427the aerosol volume over the entire range of OH exposures used in the experiment.

428

#### 429IV. Discussion

430It is clear from Figures 2, 3, 4, 6, and 7 that the Scenario 3 predictions, involving simultaneous  
431free radical and acid-base OH oxidation channels with fragmentation and volatilization, correctly  
432describe the observed trends in volume, composition and reactivity as a function of OH  
433exposure. Comparison of the Scenario predictions reveals that OH-abstraction initiates free  
434radical reactions that functionalize the carbon skeleton, while OH reactions with carboxylate  
435groups arising from acid-base chemistry activate carbon-carbon bond scission in alkoxy radicals,  
436leading to the formation of low molecular weight, highly oxidized products such as malic and  
437mesoxalic acid. The extensive fragmentation predicted by Scenarios 2 and 3 is consistent with  
438the results of previous studies of oxidation of highly oxidized aerosol as discussed in the  
439Introduction, suggesting that carboxylate formation is a key species that drives aerosol  
440volatilization. As more highly oxidized products are formed, they accrete water, which causes the  
441substantial initial volume growth observed to accompany oxidation. The decrease in volume, at  
442larger OH exposures, originates from the formation and subsequent evaporation of volatile C<sub>2</sub>  
443reaction products along with their waters of solvation into the gas phase, which is held at 62.5%

444RH. These results highlight the significant role of water in controlling not only changes in  
445physical properties but also the mechanisms of oxidation and fragmentation of aerosol  
446components in the atmosphere.

447

448The importance of including coupled acid-base/free radical reaction pathways is primarily  
449revealed by predictions of aerosol composition, since there are no clear features in the CA decay  
450kinetics or the average O/C and H/C to indicate that more than free radical chemistry is occurring  
451(i.e. all scenario predictions compare favorably with experiment within the error). Rather, a  
452primary signature of acid-base chemistry is found in the formation of a specific product:  
453mesoxalic acid ( $m/z = 116.98$ ), which is the most abundant product in CA oxidation. The specific  
454reaction channel controlling the formation of this  $C_3$  diacid is the rate at which acyloxy radicals  
455form from carboxyl groups. This can occur *via* two distinct pathways: (1) the H atom abstraction  
456from a carboxylic acid group by OH and (2) the OH charge transfer reaction at a carboxylate  
457group. Figure 8 compares the rate coefficients for these channels,<sup>67-68</sup> showing that  $k$  for the  
458charge transfer pathway is 80 times larger. This explains the simulation predictions using  
459Scenario 1, which lacks acid/base chemistry. In Scenario 1, the acyloxy radical formation  
460channel, and hence fragmentation, is less important because it is slower than other competing  
461hydrogen abstraction reactions (e.g. H atom abstraction from a  $-CH_2$  group). The lack of  
462carboxylate species in Scenario 1 eliminates the additional carboxylic acid formation pathways  
463shown in Figure 9. These pathways, which involve fragmentation and decrease carboxylic acid  
464carbons numbers by 1, account for over 90% of the total malonic acid ( $C_3H_4O_4$ ) production in the  
465model. As shown in Figure 10, malonic acid is a critical precursor for mesoxalic acid. OH  
466radical abstraction from malonic acid followed by  $O_2$  addition forms a peroxy radical which can

467then react with  $\text{RO}_2$  or  $\text{HO}_2$  to yield mesoxalic acid. The simulations suggest that the  $\text{RO}_2$  and  
468 $\text{HO}_2$  pathways to form mesoxalic acid are equally important.

469

470The decarboxylation pathway (Figure 9), is operative only in those Scenarios that include acid  
471-base chemistry (Scenarios 2 and 3) and is the major source of  $\text{C}_3$  products generated by  $\text{CO}_2$   
472elimination from  $\text{C}_4$  species. This is clearly seen in the carbon number plot in Figure 11, where  
473Scenario 1 produces mainly  $\text{C}_4$  products and only very small quantities of  $\text{C}_3$  reaction products,  
474unlike Scenarios 2 and 3 (which include carboxylate pathways) and the experimental  
475observations.

476

477As seen in Figure 11, another notable difference between Scenario 1 and Scenarios 2 and 3 is the  
478production rate of  $\text{C}_5$  products, which are observed in the experiments. This result can be  
479explained by the relative barrier heights for alkoxy radical decomposition. As shown in Figure  
48012, H atom abstraction by OH from the alcohol group of CA forms an alkoxy radical adjacent to  
481a carboxyl functionality. The subsequent unimolecular fragmentation rate of the alkoxy radical  
482anion in aqueous solution is many orders of magnitude faster than that of its neutral form,  
483particularly if a carboxylate forms during the C-C bond rupture. Accordingly, the resulting  $\text{C}_5$   
484product,  $\beta$ -ketoglutaric acid ( $\text{C}_5\text{H}_6\text{O}_5$ ), which is observed experimentally is only produced in  
485Scenarios 2 and 3 (Figure 11) via reaction pathways involving the conjugate base of CA. When  
486acid-base chemistry is absent (i.e. Scenario 1) this particular fragmentation pathway is of minor  
487importance because it is slow relative to other possible alkoxy radical reactions. Interestingly, the  
488differences in product distributions due to the presence or absence of acid-base chemistry have a  
489negligible impact on the predicted van Krevelen diagrams. This suggests that average aerosol

490elemental composition, not surprisingly, is a blunt probe of the underlying elementary reaction  
491pathways.

492

493The acyloxy reaction pathway shown in Figure 9 is the direct route to transform mesoxalic acid  
494into oxalic acid. Oxalic acid, the most abundant atmospheric particulate organic diacid, has  
495temporally varying concentrations (seasonal and diurnal) that suggest its abundance is controlled  
496by secondary processes.<sup>69-72</sup> Indeed, field measurements of oxalic acid support an in-cloud  
497formation mechanism.<sup>73-74</sup> In model scenarios 2 and 3, oxalic acid is the most abundant acid in  
498the system by the end of the simulation runs. Thus, the activation of the carboxylate group  
499towards acyloxy radical formation and its subsequent reactions as shown in Figures 8 and 9  
500provide a possible mechanism for oxalic acid formation in the atmosphere.

501

502The aerosol volumes (Figure 7) predicted in Scenarios 1 and 2 continuously increase over time,  
503in contrast to Scenario 3 (and the experiment), which exhibit a maximum. This is not surprising  
504since only Scenario 3 allows for the production of reaction products that partition to the gas  
505phase resulting in a net decrease of material in the aerosol. In particular, we find that C<sub>2</sub> product  
506evaporation is the most important contributor to the observed decrease in aerosol volume. The  
507large increase in aerosol volume at early OH exposures can be explained by an increase of  
508aerosol hygroscopicity due to the increase in the total quantity of soluble molecules (i.e.  
509fragmentation products) originating from the extensive C-C bond scission chemistry discussed  
510above. This initial increase is much steeper for Scenario 2 than 1 and can be explained by the  
511larger population of C<sub>3</sub> and C<sub>5</sub> fragmentation products (Figure 11) produced in Scenario 2 via the  
512carboxylate reactions discussed above.



513

514 Finally, in all three scenarios, ROOH photolysis is found to be a negligible reaction pathway. In  
515 the simulations, photolysis occurs on average once for every 20,000  $\beta$ -scission reactions. Rather,  
516 the main sink for ROOH is C-H attack by OH, as shown in Figure 13, which functionalizes the  
517 carbon skeleton with a ketone group. Subsequent hydration, hydrogen abstraction from the  
518 hydroxyl group, and fragmentation yields oxaloacetic acid ( $C_4H_4O_5$ ), the key  $C_4$  product  
519 undergoing the carboxyl-forming pathway in Figure 9. Thus, ketone production from ROOH  
520 reaction with OH is a major contributor to eventual  $C_3$  product formation. This is only possible  
521 when acid-base chemistry activates acyloxy radical formation.

522

## 523 V. Conclusion

524 A detailed, physically based kinetics model is formulated for the heterogeneous oxidation of  
525 aqueous citric acid aerosol by OH. Citric acid is a reasonable proxy for understanding the  
526 fundamental chemical pathways that might be important for prediction of secondary organic  
527 aerosol and late-stage aging of primary aerosol in the troposphere. We find that substantial  
528 coupling of acid-base and free radical chemistry is needed to explain the heterogeneous  
529 oxidation of CA by OH, and that carboxylate groups are central to trends in aerosol composition  
530 and size observed as a function of OH exposure. When present in carboxylic acid form only,  
531 reactions with OH lead mainly to functionalization of CA. When neutral CA is equilibrated with  
532 its conjugate base, extensive fragmentation occurs following H abstraction. Larger carbon  
533 numbered diacids are transformed into smaller diacids through the interplay of acid-base and free  
534 radical chemistry, activating acyloxy formation and driving subsequent decarboxylation and  
535 carboxyl-group formation. In addition, the carboxylate group significantly lowers the barrier

536height to C-C bond scission in alkoxy radicals. Together, these two effects of acid-base chemistry  
537are essential to simultaneously predict the kinetic decay of citric acid, changes in aerosol volume,  
538and the product distribution within the aerosol. The presence of mesoxalic acid as a product is a  
539key signature of acid-base chemistry in this system; reaction rates and elemental compositions  
540alone do not provide evidence that this reaction channel is occurring. The simulation results also  
541provide insight to how elementary reaction steps controls the evolution of aerosol size during  
542oxidation. The detailed trend is controlled by a subtle balance of chemical erosion and  
543hygroscopic growth.

544

545How does this fit in with what is known about aerosol ageing processes? As shown by Lambe et  
546al.,<sup>75</sup> the quantity of secondary aerosol formed by the reaction of OH with alkanes evolves  
547dynamically by functionalization and fragmentation.<sup>3</sup> Functionalization dominates early stage  
548oxidation and leads to substantial aerosol yield. At higher oxidation levels, the aerosol yield  
549reaches a maximum, and further reaction reduces the quantity of aerosol by the production of gas  
550phase products (i.e. fragmentation). Carboxylic acids are expected to be key particle phase  
551products that contribute substantially to lowering aerosol volatility (i.e. enhancing the quantity of  
552aerosol) while raising its oxidation state and hygroscopicity. Our results suggest a new  
553connection between aerosol pH and water that may govern the balance of functionalization and  
554fragmentation in aqueous secondary organic aerosol. As the oxidation state of the aerosol  
555increases by the formation of acids, water uptake naturally follows, opening acid-base reaction  
556channels. This indicates that carboxylic acids could play a dual role. At early stages, these highly  
557oxidized species mainly contribute to increase in aerosol mass and water uptake. When the

558character of the aerosol becomes aqueous, acid-base equilibria lead to an increase in carboxylate-  
559mediated chemistry which largely consists of C-C bond scission reactions (i.e. chemical erosion).

560

561Here we have considered only a single relative humidity (RH = 64.5%) where the aerosol is a  
562well-mixed aqueous solution on the timescale of the OH reaction frequency. We expect more  
563complex behavior to appear as the RH is lowered and the aerosol and its subsequent  
564transformations are governed increasingly by nanoscale interfacial gradients produced by slow  
565diffusional timescales in the particle.<sup>8, 37</sup> For these cases we might expect much more complex  
566feedbacks to emerge between aerosol viscosity and hygroscopicity and the underlying  
567elementary free radical and acid-base reaction pathways.

568

### 569**Supporting Information**

570Model construction; Structures, pKa, Kh and densities of organic acid species used in  
571simulations; Validation of implicit acid-base modeling (explicit acid-base model results);  
572Comparison of scenario 3 mass spectrum with experiment; Sample Gaussian09 results for alkoxy  
573radical anion ground state and transition state; Evaluation of sensitivity of the simulation results  
574for Scenario 3 with faster peroxy-peroxy kinetics

575

### 576**Acknowledgements**

577This paper is based upon work supported by the Laboratory Directed Research and Development  
578Program of the Department of Energy's Lawrence Berkeley National Laboratory under U. S.  
579Department of Energy Office of Science, Office of Basic Energy Sciences, Chemical Sciences,  
580Geosciences, and Biosciences Division, under Contract No. DE-AC02-05CH11231. Results were

581used from past K. R. W. work supported by the Department of Energy's Office of Science Early  
582Career Research Program and by Chemical Sciences, Geosciences, and Biosciences Division of  
583the U. S. Department of Energy under Contract No. DE-AC02-05CH11231. M. J. L. sincerely  
584thanks the Cal Energy Corps for a summer internship (2015), during which he started this  
585research project. M. J. L. was supported during the summer of 2016 by the Chemical Sciences  
586Division (BES Early Career Award to K.R.W.) of the U. S. Department of Energy under Contract  
587No. DE-AC02-05CH11231. M. J. L. thanks Professor Ronald Cohen (UC Berkeley) for serving  
588as faculty sponsor to continue his research during the academic year. The authors are grateful to  
589Professor Jason Goodpaster (University of Minnesota) for his assistance in conducting ab-initio  
590calculations, to Dr. James Davies for providing data, and to Dr. William Hinsberg (Columbia Hill  
591Technical Consulting) for his advice on several aspects of Kinetiscope use in this work.

592

### 593References

594

5951. Buseck, P. R.; Pósfai, M., Airborne minerals and related aerosol particles: Effects on  
596climate and the environment. *Proceedings of the National Academy of Sciences of the United*  
597*States of America* **1999**, *96*, 3372-3379.
5982. Burkholder, J.; Abbatt, J.; Barnes, I.; Roberts, J.; Melamed, M.; Ammann, M.; Bertram,  
599A.; Cappa, C.; Carlton, A. M.; Carpenter, L. J., The essential role for laboratory studies in  
600atmospheric chemistry. *Environmental Science and Technology* **2017**.
6013. Kroll, J. H.; Smith, J. D.; Che, D. L.; Kessler, S. H.; Worsnop, D. R.; Wilson, K. R.,  
602Measurement of fragmentation and functionalization pathways in the heterogeneous oxidation of  
603oxidized organic aerosol. *Physical Chemistry Chemical Physics* **2009**, *11*, 8005-8014.
6044. George, I. J.; Abbatt, J. P. D., Heterogeneous oxidation of atmospheric aerosol particles  
605by gas-phase radicals. *Nature chemistry* **2010**, *2*, 713-722.
6065. George, I. J.; Slowik, J.; Abbatt, J. P. D., Chemical aging of ambient organic aerosol from  
607heterogeneous reaction with hydroxyl radicals. *Geophysical Research Letters* **2008**, *35*.
6086. Kolesar, K. R.; Buffaloe, G.; Wilson, K. R.; Cappa, C. D., OH-initiated heterogeneous  
609oxidation of internally-mixed squalane and secondary organic aerosol. *Environmental Science*  
610*and Technology* **2014**, *48*, 3196-3202.

6117. Nah, T.; Kessler, S. H.; Daumit, K. E.; Kroll, J. H.; Leone, S. R.; Wilson, K. R., OH-  
612initiated oxidation of sub-micron unsaturated fatty acid particles. *Physical Chemistry Chemical  
613Physics* **2013**, *15*, 18649-63.
6148. Wiegel, A. A.; Liu, M.; Hinsberg, W. D.; Wilson, K. R.; Houle, F. A., Diffusive  
615confinement of free radical intermediates in the OH radical oxidation of semisolid aerosol.  
616*Physical Chemistry Chemical Physics* **2017**, *19*, 6814-6830.
6179. Herrmann, H., Kinetics of aqueous phase reactions relevant for atmospheric chemistry.  
618*Chemical Reviews* **2003**, *103*, 4691-4716.
61910. Herrmann, H.; Schaefer, T.; Tilgner, A.; Styler, S. A.; Weller, C.; Teich, M.; Otto, T.,  
620Tropospheric aqueous-phase chemistry: kinetics, mechanisms, and its coupling to a changing gas  
621phase. *Chemical Reviews* **2015**, *115*, 4259-4334.
62211. Blando, J. D.; Turpin, B. J., Secondary organic aerosol formation in cloud and fog  
623droplets: A literature evaluation of plausibility. *Atmospheric Environment* **2000**, *34*, 1623-1632.
62412. Ervens, B.; Feingold, G.; Frost, G. J.; Kreidenweis, S. M., A modeling of study of  
625aqueous production of dicarboxylic acids: 1. Chemical pathways and speciated organic mass  
626production. *Journal of Geophysical Research D: Atmospheres* **2004**, *109*, 1-20.
62713. Marais, E. A.; Jacob, D. J.; Jimenez, J. L.; Campuzano-Jost, P.; Day, D. A.; Hu, W.;  
628Krechmer, J.; Zhu, L.; Kim, P. S.; Miller, C. C.; et al, Aqueous-phase mechanism for secondary  
629organic aerosol formation from isoprene: application to the southeast United States and co-  
630benefit of SO<sub>2</sub> emission controls. *Atmos. Chem. Phys.* **2016**, *16*, 1603-1618.
63114. Lim, Y. B.; Tan, Y.; Perri, M. J.; Seitzinger, S. P.; Turpin, B. J., Aqueous chemistry and its  
632role in secondary organic aerosol (SOA) formation. *Atmos. Chem. Phys.* **2010**, *10*, 10521-10539.
63315. Schone, L.; Schindelka, J.; Szeremeta, E.; Schaefer, T.; Hoffmann, D.; Rudzinski, K. J.;  
634Szmigielski, R.; Herrmann, H., Atmospheric aqueous phase radical chemistry of the isoprene  
635oxidation products methacrolein, methyl vinyl ketone, methacrylic acid and acrylic acid -  
636kinetics and product studies. *Physical Chemistry Chemical Physics* **2014**, *16*, 6257-6272.
63716. Chan, M. N.; Zhang, H. F.; Goldstein, A. H.; Wilson, K. R., Role of water and phase in  
638the heterogeneous oxidation of solid and aqueous succinic acid aerosol by hydroxyl radicals.  
639*Journal of Physical Chemistry C* **2014**, *118*, 28978-28992.
64017. Cheng, C. T.; Chan, M. N.; Wilson, K. R., The role of alkoxy radicals in the  
641heterogeneous reaction of two structural isomers of dimethylsuccinic acid. *Physical Chemistry  
642Chemical Physics* **2015**, *17*, 25309-25321.
64318. Cheng, C. T.; Chan, M. N.; Wilson, K. R., Importance of unimolecular HO<sub>2</sub> elimination  
644in the heterogeneous OH reaction of highly oxygenated tartaric acid aerosol. *Journal of Physical  
645Chemistry A* **2016**, *120*, 5887-5896.

64619. Kessler, S. H.; Nah, T.; Daumit, K. E.; Smith, J. D.; Leone, S. R.; Kolb, C. E.; Worsnop, D. R.; Wilson, K. R.; Kroll, J. H., OH-initiated heterogeneous aging of highly oxidized organic aerosol. *Journal of Physical Chemistry A* **2012**, *116*, 6358-6365.
64920. Kessler, S. H.; Smith, J. D.; Che, D. L.; Worsnop, D. R.; Wilson, K. R.; Kroll, J. H., Chemical sinks of organic aerosol: Kinetics and products of the heterogeneous oxidation of erythritol and levoglucosan. *Environmental Science and Technology* **2010**, *44*, 7005-7010.
65221. Slade, J. H.; Knopf, D. A., Heterogeneous OH oxidation of biomass burning organic aerosol surrogate compounds: assessment of volatilisation products and the role of OH concentration on the reactive uptake kinetics. *Physical Chemistry Chemical Physics* **2013**, *15*, 5898-915.
65622. Slade, J. H.; Knopf, D. A., Multiphase OH oxidation kinetics of organic aerosol: The role of particle phase state and relative humidity. *Geophysical Research Letters* **2014**, *41*, 5297-5306.
65823. Slade, J. H.; Shiraiwa, M.; Arangio, A.; Su, H.; Pöschl, U.; Wang, J.; Knopf, D. A., Cloud droplet activation through oxidation of organic aerosol influenced by temperature and particle phase state. *Geophysical Research Letters* **2017**, *44*, 1583-1591.
66124. Harmon, C. W.; Ruehl, C. R.; Cappa, C. D.; Wilson, K. R., A statistical description of the evolution of cloud condensation nuclei activity during the heterogeneous oxidation of squalane and bis(2-ethylhexyl) sebacate aerosol by hydroxyl radicals. *Physical Chemistry Chemical Physics* **2013**, *15*, 9679-9693.
66525. George, I.; Chang, R.-W.; Danov, V.; Vlasenko, A.; Abbatt, J., Modification of cloud condensation nucleus activity of organic aerosols by hydroxyl radical heterogeneous oxidation. *Atmospheric Environment* **2009**, *43*, 5038-5045.
66826. Kroll, J. H.; Donahue, N. M.; Jimenez, J. L.; Kessler, S. H.; Canagaratna, M. R.; Wilson, K. R.; Altieri, K. E.; Mazzoleni, L. R.; Wozniak, A. S.; Bluhm, H.; et al, Carbon oxidation state as a metric for describing the chemistry of atmospheric organic aerosol. *Nature Chemistry* **2011**, *3*, 133-139.
67227. Hoffmann, D.; Tilgner, A.; Iinuma, Y.; Herrmann, H., Atmospheric stability of levoglucosan: a detailed laboratory and modeling study. *Environmental Science & Technology* **2010**, *44*, 694-699.
67528. Zhao, R.; Mungall, E. L.; Lee, A. K. Y.; Aljawhary, D.; Abbatt, J. P. D., Aqueous-phase photooxidation of levoglucosan-A mechanistic study using aerosol time-of-flight chemical ionization mass spectrometry (Aerosol ToF-CIMS). *Atmospheric Chemistry and Physics* **2014**, *14*, 9695-9705.
67929. Hennigan, C. J.; Sullivan, A. P.; Collett, J. L.; Robinson, A. L., Levoglucosan stability in biomass burning particles exposed to hydroxyl radicals. *Geophysical Research Letters* **2010**, *37*, L09806.

68230. Daumit, K. E.; Carrasquillo, A. J.; Hunter, J. F.; Kroll, J. H., Laboratory studies of the aqueous-phase oxidation of polyols: Submicron particles vs. bulk aqueous solution. *Atmospheric Chemistry and Physics* **2014**, *14*, 10773-10784.
68531. Wiegel, A. A.; Wilson, K. R.; Hinsberg, W. D.; Houle, F. A., Stochastic methods for aerosol chemistry: a compact molecular description of functionalization and fragmentation in the heterogeneous oxidation of squalane aerosol by OH radicals. *Physical Chemistry Chemical Physics* **2015**, *17*, 4398-4411.
68932. Enami, S.; Hoffmann, M. R.; Colussi, A. J., In situ mass spectrometric detection of interfacial intermediates in the oxidation of RCOOH(aq) by gas-phase OH-radicals. *Journal of Physical Chemistry A* **2014**, *118* (23), 4130-4137.
69233. Enami, S.; Hoffmann, M. R.; Colussi, A. J., OH-radical specific addition to glutathione S-atom at the air-water interface: relevance to the redox balance of the lung epithelial lining fluid. *Journal of Physical Chemistry Letters* **2015**, *6* (19), 3935-3943.
69534. Enami, S.; Hoffmann, M. R.; Colussi, A. J., Stepwise oxidation of aqueous dicarboxylic acids by gas-phase OH radicals. *Journal of Physical Chemistry Letters* **2015**, *6* (3), 527-534.
69735. Enami, S.; Sakamoto, Y., OH-radical oxidation of surface-active cis-pinonic acid at the air-water interface. *Journal of Physical Chemistry A* **2016**, *120* (20), 3578-3587.
69936. Kameel, F. R.; Riboni, F.; Hoffmann, M. R.; Enami, S.; Colussi, A. J., Fenton oxidation of gaseous isoprene on aqueous surfaces. *Journal of Physical Chemistry C* **2014**, *118* (50), 29151-29158.
70237. Davies, J. F.; Wilson, K. R., Nanoscale interfacial gradients formed by the reactive uptake of OH radicals onto viscous aerosol surfaces. *Chem. Sci.* **2015**, *6*, 7020-7027.
70438. Gillespie, D. T., Stochastic simulation of chemical kinetics. *Annual Review of Physical Chemistry* **2007**, *58*, 35-55.
70639. Hinsberg, W. D.; Houle, F. A., *Kinetiscope*. Columbia Hill Technical Consulting: Fremont, CA: [www.hinsberg.net/kinetiscope](http://www.hinsberg.net/kinetiscope), 2015.
70840. Bunker, D. L.; Garrett, B.; Kleindienst, T.; Long, G. S., Discrete simulation methods in combustion kinetics. *Combust Flame* **1974**, *23* (3), 373-379.
71041. Gillespie, D. T., General method for numerically simulating stochastic time evolution of coupled chemical reactions. *J Comput Phys* **1976**, *22* (4), 403-434.
71242. Wallraff, G.; Hutchinson, J.; Hinsberg, W.; Houle, F.; Seidel, P.; Johnson, R.; Oldham, W., Thermal and acid-catalyzed deprotection kinetics in candidate deep-ultraviolet resist materials. *J Vac Sci Technol B* **1994**, *12* (6), 3857-3862.

71543. Houle, F. A.; Hinsberg, W. D.; Wilson, K. R., Oxidation of a model alkane aerosol by OH 716radical: the emergent nature of reactive uptake. *Physical Chemistry Chemical Physics* **2015**, *17*, 7174412-4423.
71844. Davidovits, P.; Worsnop, D. R.; Jayne, J. T.; Kolb, C. E.; Winkler, P.; Vrtala, A.; Wagner, 719P. E.; Kulmala, M.; Lehtinen, K. E. J.; Vesala, T.; Mozurkewich, M., Mass accommodation 720coefficient of water vapor on liquid water. *Geophysical Research Letters* **2004**, *31* (22).
72145. Garrett, B. C.; Schenter, G. K.; Morita, A., Molecular simulations of the transport of 722molecules across the liquid/vapor interface of water. *Chemical Reviews* **2006**, *106* (4), 1355- 7231374.
72446. Soonsin, V.; Zardini, A. A.; Marcolli, C.; Zuend, A.; Krieger, U. K., The vapor pressures 725and activities of dicarboxylic acids reconsidered: the impact of the physical state of the aerosol. 726*Atmospheric Chemistry and Physics* **2010**, *10*, 11753-11767.
72747. Hearn, J. D.; Renbaum, L. H.; Wang, X.; Smith, G. D., Kinetics and products from 728reaction of Cl radicals with dioctyl sebacate (DOS) particles in O<sub>2</sub>: a model for radical-initiated 729oxidation of organic aerosols. *Physical Chemistry Chemical Physics* **2007**, *9*, 4803-4813.
73048. Renbaum, L. H.; Smith, G. D., The importance of phase in the radical-initiated oxidation 731of model organic aerosols: reactions of solid and liquid brassidic acid particles. *Physical 732Chemistry Chemical Physics* **2009**, *11*, 2441-2451.
73349. Frisch, M. J. T., G. W.; Schlegel, H. B.; Scuseria, G. E.; Robb, M. A.; Cheeseman, J. R.; 734Scalmani, G.; Barone, V.; Mennucci, B.; Petersson, G. A.; Nakatsuji, H.; Caricato, M.; Li, X.; 735Hratchian, H. P.; Izmaylov, A. F.; Bloino, J.; Zheng, G.; Sonnenb, D. J., *Gaussian09*. Gaussian, 736Inc.: Wallingford, CT, 2009.
73750. Marenich, A. V.; Cramer, C. J.; Truhlar, D. G., Universal solvation model based on solute 738electron density and on a continuum model of the solvent defined by the bulk dielectric constant 739and atomic surface tensions. *Journal of Physical Chemistry B* **2009**, *113*, 6378-6396.
74051. Walker, M.; Harvey, A. J. A.; Sen, A.; Dessent, C. E. H., Performance of M06, M06-2X, 741and M06-HF density functionals for conformationally flexible anionic clusters: M06 functionals 742perform better than B3LYP for a model system with dispersion and ionic hydrogen-bonding 743interactions. *Journal of Physical Chemistry A* **2013**, *117*, 12590-12600.
74452. Vereecken, L.; Peeters, J., Decomposition of substituted alkoxy radicals--part I: a 745generalized structure-activity relationship for reaction barrier heights. *Physical Chemistry 746Chemical Physics* **2009**, *11*, 9062-9074.
74753. Nah, T.; Zhang, H.; Worton, D. R.; Ruehl, C. R.; Kirk, B. B.; Goldstein, A. H.; Leone, S. 748R.; Wilson, K. R., Isomeric product detection in the heterogeneous reaction of hydroxyl radicals 749with aerosol composed of branched and linear unsaturated organic molecules. *The Journal of 750Physical Chemistry A* **2014**, *118*, 11555-11571.



75154. Francisco, J. S. M., James T.; Yu, Hua-Gen, HOCO radical chemistry. *Accounts of Chemical Research* **2010**, *43*, 1519-1526.
75355. Hart, E. J.; Henglein, A., Free radical and free atom reactions in the sonolysis of aqueous iodide and formate solutions. *The Journal of Physical Chemistry* **1985**, *89*, 4342-4347.
75556. Janik, I.; Tripathi, G. N. R., The nature of the superoxide radical anion in water. *Journal of Chemical Physics* **2013**, *139*, 014302.
75757. Milligan, D. E.; Jacox, M. E., Infrared spectrum and structure of intermediates in the reaction of OH with CO. *Journal of Chemical Physics* **1971**, *54*, 927-942.
75958. Hinsberg, W.; Houle, F. A., Stochastic simulation method for processes containing equilibrium steps. *U. S. Patent No. 5625579 (April 29)* **1997**.
76159. Rathinam, M.; Petzold, L. R.; Cao, Y.; Gillespie, D. T., Stiffness in stochastic chemically reacting systems: The implicit tau-leaping method. *Journal of Chemical Physics* **2003**, *119*, 76312784-12794.
76460. Raventos-Duran, T.; Camredon, M.; Valorso, R.; Mouchel-Vallon, C.; Aumont, B., Structure-activity relationships to estimate the effective Henry's law constants of organics of atmospheric interest. *Atmos. Chem. Phys.* **2010**, *10* (16), 7643-7654.
76761. Lambe, A. T.; Onasch, T. B.; Massoli, P.; Croasdale, D. R.; Wright, J. P.; Ahern, A. T.; Williams, L. R.; Worsnop, D. R.; Brune, W. H.; Davidovits, P., Laboratory studies of the chemical composition and cloud condensation nuclei (CCN) activity of secondary organic aerosol (SOA) and oxidized primary organic aerosol (OPOA). *Atmospheric Chemistry and Physics* **2011**, *11*, 8913-8928.
77262. Massoli, P.; Lambe, A. T.; Ahern, A. T.; Williams, L. R.; Ehn, M.; Mikkilä, J.; Canagaratna, M. R.; Brune, W. H.; Onasch, T. B.; Jayne, J. T.; et al, Relationship between aerosol oxidation level and hygroscopic properties of laboratory generated secondary organic aerosol (SOA) particles. *Geophysical Research Letters* **2010**, *37*, 1-5.
77663. Suda, S. R.; Petters, M. D.; Yeh, K.; Strollo, C.; Matsunaga, A.; Faulhaber, A.; Ziemann, P. J.; Prenni, A. J.; Carrico, C. M.; Sullivan, R. C.; et al, Influence of functional groups on organic aerosol cloud condensation nucleus activity. *Environmental science & technology* **2014**, *48*, 10182-90.
78064. Peng, C. G.; Chow, A. H. L.; Chan, C. K., Hygroscopic study of glucose, citric acid, and sorbitol using an electrodynamic balance: Comparison with UNIFAC predictions. *Aerosol Sci Tech* **2001**, *35*, 753-758.
78365. Swanson, J. M. J.; Maupin, C. M.; Chen, H.; Petersen, M. K.; Xu, J.; Wu, Y.; Voth, G. A., Proton solvation and transport in aqueous and biomolecular systems: insights from computer simulations. *The Journal of Physical Chemistry B* **2007**, *111*, 4300-4314.

78666. Sander, S. P.; Ravishankara, A. R.; Golden, D. M.; Kolb, C. E.; Kurylo, M. J.; Molina, M. 787J.; Moortgat, G. K.; Finlayson-Pitts, B. J., Chemical kinetics and photochemical data for use in 788atmospheric studies: evaluation number 14. *JPL Publication 02-25* **2003**, *14*, 1-334.
78967. Buxton, G. V.; Greenstock, C. L.; Helman, W. P.; Ross, A. B., Critical Review of rate 790constants for reactions of hydrated electrons, hydrogen atoms and hydroxyl radicals (.OH/.O-) in 791Aqueous Solution. *Journal of Physical and Chemical Reference Data* **1988**, *17*, 513-886.
79268. Doussin, J. F.; Monod, A., Structure-activity relationship for the estimation of OH- 793oxidation rate constants of carbonyl compounds in the aqueous phase. *Atmospheric Chemistry 794and Physics Discussions* **2013**, *13*, 15949-15991.
79569. Kawamura, K.; Kasukabe, H.; Barrie, L. A., Source and reaction pathways of 796dicarboxylic acids, ketoacids and dicarbonyls in arctic aerosols: One year of observations. 797*Atmospheric Environment* **1996**, *30*, 1709-1722.
79870. Kawamura, K.; Yasui, O., Diurnal changes in the distribution of dicarboxylic acids, 799ketocarboxylic acids and dicarbonyls in the urban Tokyo atmosphere. *Atmospheric Environment* 800**2005**, *39*, 1945-1960.
80171. Mochida, M.; Umemoto, N.; Kawamura, K.; Uematsu, M., Bimodal size distribution of 802C-2-C-4 dicarboxylic acids in the marine aerosols. *Geophysical Research Letters* **2003**, *30*, 1672.
80372. Rogge, W. F.; Mazurek, M. A.; Hildemann, L. M.; Cass, G. R.; Simoneit, B. R. T., 804Quantification of urban organic aerosols at a molecular level: Identification, abundance and 805seasonal variation. *Atmospheric Environment Part A, General Topics* **1993**, *27*, 1309-1330.
80673. Crahan, K. K.; Hegg, D.; Covert, D. S.; Jonsson, H., An exploration of aqueous oxalic 807acid production in the coastal marine atmosphere. *Atmospheric Environment* **2004**, *38*, 3757- 8083764.
80974. Yu, J. Z.; Huang, X.-F.; Xu, J.; Hu, M., When aerosol sulfate goes up, so does oxalate: 810implication for the formation mechanisms of oxalate. *Environmental science & technology* **2005**, 811**39**, 128-133.
81275. Lambe, A. T.; Onasch, T. B.; Croasdale, D. R.; Wright, J. P.; Martin, A. T.; Franklin, J. P.; 813Massoli, P.; Kroll, J. H.; Canagaratna, M. R.; Brune, W. H. e. a., Transitions from 814functionalization to fragmentation reactions of laboratory secondary organic aerosol (SOA) 815generated from the OH oxidation of alkane precursors. *Environmental Science & Technology* 816**2012**, *46*, 5430-5437.
81776. Denisov, E. T.; Afanas'ev, I. B., *Oxidation and Antioxidants in Organic Chemistry and 818Biology*. Taylor & Francis: Boca Raton, FL, 2005.
81977. Sander, R., Compilation of Henry's law constants (version 4.0) for water as solvent. 820*Atmos. Chem. Phys.* **2015**, *15*, 4399-4981.

82178. Doussin, J. F.; Monod, A., Structure–activity relationship for the estimation of OH-oxidation rate constants of carbonyl compounds in the aqueous phase. *Atmos. Chem. Phys.* **2013**, *13*, 11625-11641.

82479. Monod, A.; Doussin, J. F., Structure-activity relationship for the estimation of OH-oxidation rate constants of aliphatic organic compounds in the aqueous phase: alkanes, alcohols, organic acids and bases. *Atmospheric Environment* **2008**, *42*, 7611-7622.

82780. Sander, S. P. G., D. M.; Kurylo, M. J.; Moortgat, G. K.; Wine, P. H.; Ravishankara, A. R.; Kolb, C. E.; Molina, M. J.; Finlayson-Pitts, B. J.; Huie, R. E.; et al, Chemical kinetics and photochemical data for use in atmospheric studies evaluation number 15. *JPL Publication 06-2* **2006**, *15*, 1-523.

83181. Atkinson, R.; Baulch, D. L.; Cox, R. A.; Crowley, J. N.; Hampson, R. F.; Hynes, R. G.; Jenkin, M. E.; Rossi, M. J.; Troe, J., Evaluated kinetic and photochemical data for atmospheric chemistry: Volume I - gas phase reactions of Ox, HOx, NOx and SOx species. *Atmos. Chem. Phys.* **2004**, *4*, 1461-1738.

83582. Wallington, T. J.; Dagaut, P.; Kurylo, M. J., UV absorption cross sections and reaction kinetics and mechanisms for peroxy radicals in the gas phase. *Chemical Reviews* **1992**, *92*, 667-710.

83883. Vaghjiani, G. L.; Ravishankara, A. R., Kinetics and mechanism of hydroxyl radical reaction with methyl hydroperoxide. *The Journal of Physical Chemistry* **1989**, *93*, 1948-1959.

840

841

842

843

844 **Table 1: Key Model Parameters and Rate Coefficients**

845

Parameter	Value	Description and References
<i>RH</i>	64.5%	Relative Humidity
<i>d<sub>p</sub></i>	97 nm	Diameter of particle
<i>k<sub>ad</sub></i>	0.052 s <sup>-1</sup>	Pseudo-first order adsorption rate coefficient of OH
[OH]	7.5 × 10 <sup>10</sup> molec. cm <sup>-3</sup>	Average experimental [OH] <sup>37</sup>
<i>k<sub>RO2+O2</sub></i>	2.0 × 10 <sup>5</sup> s <sup>-1</sup>	Pseudo-first order reaction rate coefficient of RO <sub>2</sub> + O <sub>2</sub> <sup>a</sup>
<i>k<sub>photolysis</sub></i>	1.3 × 10 <sup>-4</sup> s <sup>-1</sup>	Rate coefficient of ROOH photolysis (see text for details)
<i>k<sub>CA(CH2)+OH</sub></i>	5.1 × 10 <sup>-14</sup> cm <sup>3</sup> molecules <sup>-1</sup> s <sup>-1</sup>	Rate coefficient of H abstraction from -CH <sub>2</sub> group in CA <sup>b</sup>
<i>k<sub>CA(OH)+OH</sub></i>	9.7 × 10 <sup>-14</sup> cm <sup>3</sup> molecules <sup>-1</sup> s <sup>-1</sup>	Rate coefficient of H abstraction from -OH group in CA <sup>b</sup>
<i>k<sub>RO2+HO2</sub></i>	3.8 × 10 <sup>-15</sup> cm <sup>3</sup> molecules <sup>-1</sup> s <sup>-1</sup>	Rate coefficient of RO <sub>2</sub> + HO <sub>2</sub> <sup>c</sup>
<i>k<sub>ROOH+OH</sub></i>	3.7 × 10 <sup>-12</sup> cm <sup>3</sup> molecules <sup>-1</sup> s <sup>-1</sup>	Rate coefficient of ROOH + OH <sup>d</sup>
<i>k<sub>RO2+RO2</sub></i>	1.6 × 10 <sup>-15</sup> cm <sup>3</sup> molecules <sup>-1</sup> s <sup>-1</sup>	Rate coefficient of RO <sub>2</sub> + RO <sub>2</sub> <sup>76</sup>
<i>k<sub>RCOOH+OH</sub></i>	2.3 × 10 <sup>-15</sup> cm <sup>3</sup> molecules <sup>-1</sup> s <sup>-1</sup>	Rate coefficient of RCOOH + OH <sup>e, 67</sup>
<i>k<sub>RCOO+OH</sub></i>	2.0 × 10 <sup>-13</sup> cm <sup>3</sup> molecules <sup>-1</sup> s <sup>-1</sup>	Rate coefficient of RCOO- + OH <sup>68</sup>
<i>k<sub>HO2+OH</sub></i>	1.7 × 10 <sup>-11</sup> cm <sup>3</sup> molecules <sup>-1</sup> s <sup>-1</sup>	Rate coefficient of HO <sub>2</sub> + OH <sup>66</sup>
<i>k<sub>HO2+HO2</sub></i>	1.7 × 10 <sup>-15</sup> cm <sup>3</sup> molecules <sup>-1</sup> s <sup>-1</sup>	Rate coefficient of HO <sub>2</sub> + HO <sub>2</sub> <sup>66</sup>
<i>K<sub>hydration</sub></i>	Structure activity relationships	Equilibrium Constant for R=O ↔ R(OH) <sub>2</sub> <sup>f</sup>

846<sup>a</sup> Pseudo first order rate coefficient was computed using the Henry's Law constant<sup>77</sup> of 0.0138 and a rate coefficient<sup>76</sup> for RO<sub>2</sub> + O<sub>2</sub> of 2.5 × 10<sup>-12</sup> cm<sup>3</sup> molec<sup>-1</sup> s<sup>-1</sup>

848<sup>b</sup> Computed via structure activity relationships described in Refs. <sup>78-79</sup> Values for all the other species in the reaction (Table S1 in the SI) are similarly calculated and fall in the range of 10<sup>-14</sup> – 10<sup>-13</sup> cm<sup>3</sup> molecules<sup>-1</sup> s<sup>-1</sup>.

851<sup>c</sup> The RO<sub>2</sub> + HO<sub>2</sub> rate coefficient in the aqueous phase is estimated using the 2-3 times difference in the rate coefficient<sup>80</sup> from HO<sub>2</sub> + HO<sub>2</sub> observed in the gas phase.<sup>81-82</sup> Peroxy-peroxy rate coefficients in solution can span a large range, and the values used here are at the lower end of the range. The sensitivity of the results to values set to the high end of the range is discussed in the SI (See section S6, Scenario 4).

855<sup>d</sup> Rate coefficient used is consistent with values (~ 10<sup>-12</sup> cm<sup>3</sup> molec<sup>-1</sup> s<sup>-1</sup>) reported in Refs. <sup>80, 83</sup>

856<sup>e</sup> This rate coefficient is that for abstraction of H from the carboxylic acid group in oxalic acid.

857<sup>f</sup> The equilibrium constants for hydration reactions were calculated from the structure activity relationships and are listed in Table S1 in the SI. (see Ref. <sup>60</sup>) As described for acid-base chemistry, this equilibrium constant was folded into an effective rate constant.

860

69

35

70

861

862

863

864

865

866**Table 2: Model Scenarios**

Scenario	Free Radical	Acid-Base	Evaporation of C <sub>2</sub> Fragments
1	✓	✗	✗
2	✓	✓	✗
3	✓	✓	✓

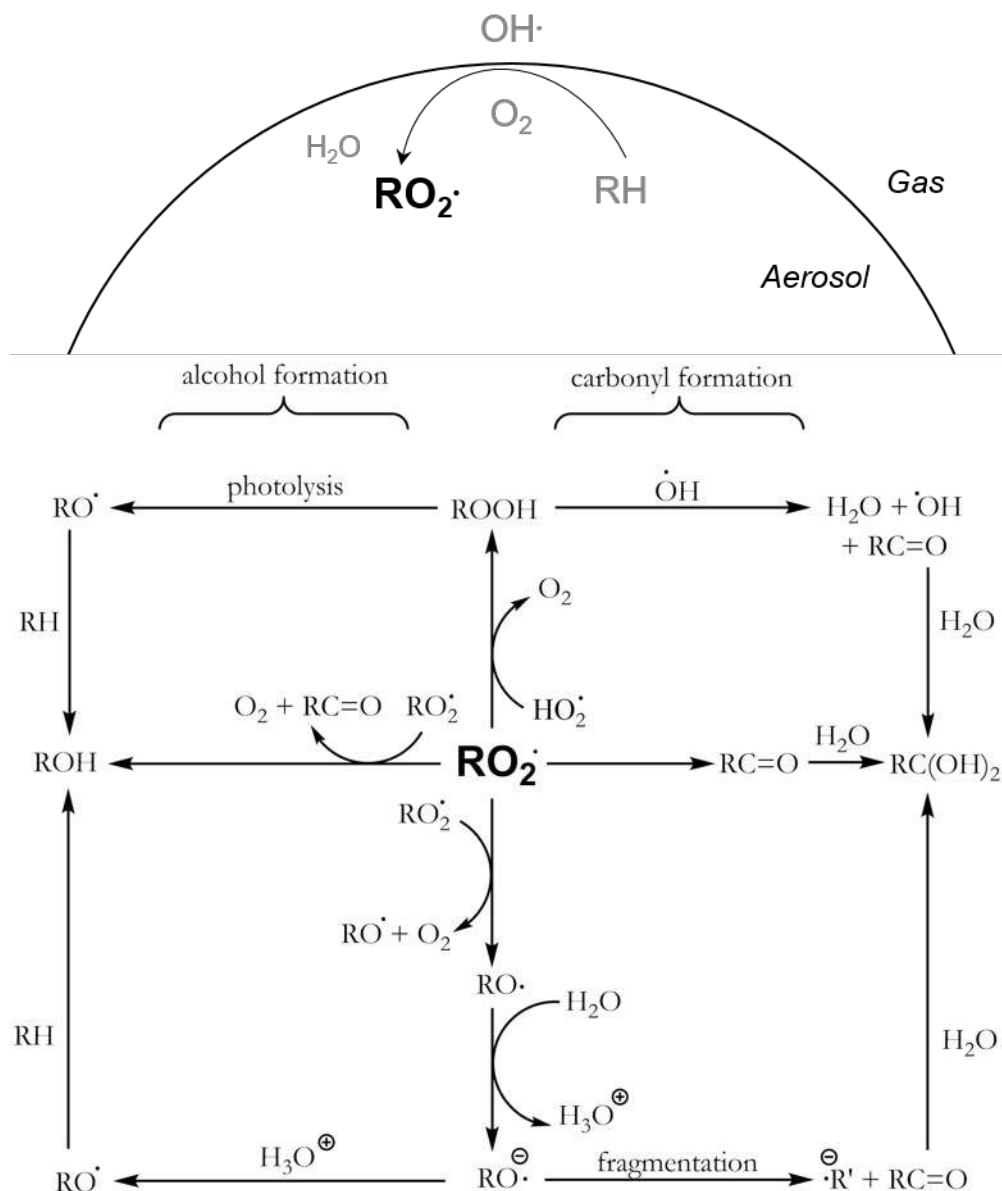
869**Table 3: Decay Constant Comparison:** Experimental and simulated reaction rate constant of  
 870CA. Coefficient of determination values ( $R^2$ ) are calculated for the model scenarios to validate  
 871the exponential fit. Note that only scenario 3 has a reaction rate constant value within  
 872experimental error.

873

<i>Model Scenario</i>	$k_{obs}$ ( $cm^3 s^{-1} molec^{-1}$ )	$R^2$
<i>Experiment</i>	$(5.27 \pm 0.28) \times 10^{-13}$	
1	$4.68 \times 10^{-13}$	.99
2	$6.08 \times 10^{-13}$	.99
3	$5.38 \times 10^{-13}$	.99

874

875



876

877**Figure 1:** Reaction pathways of  $RO_2$  to yield functionalized and/or fragmented products. A  
 878diagram of the free radical, pathways of  $RO_2$  and subsequent acid-base and hydration reactions  
 879used to model the heterogeneous oxidation of aqueous citric acid aerosol by  $OH$  radicals. The  
 880left and right branches of the  $RO_2$  reactions generate functionalized organic products. The top and  
 881bottom branches not only promote free radical cycling, but lead to bond cleaving reactions that  
 882produce lower weight, more functionalized reaction products. The  $RO$  fragmentation channel is  
 883significantly activated by an adjacent functional group and/or the deprotonation of a carboxyl  
 884group in the radical, as suggested by *ab initio* calculations (see text for details).

885

886

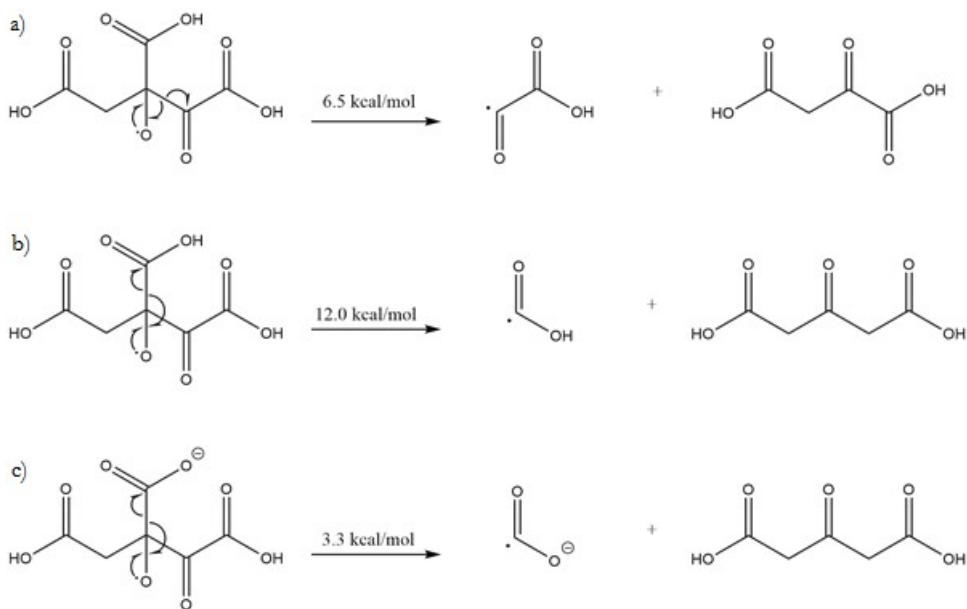
887

888

889

890

## Scheme 1

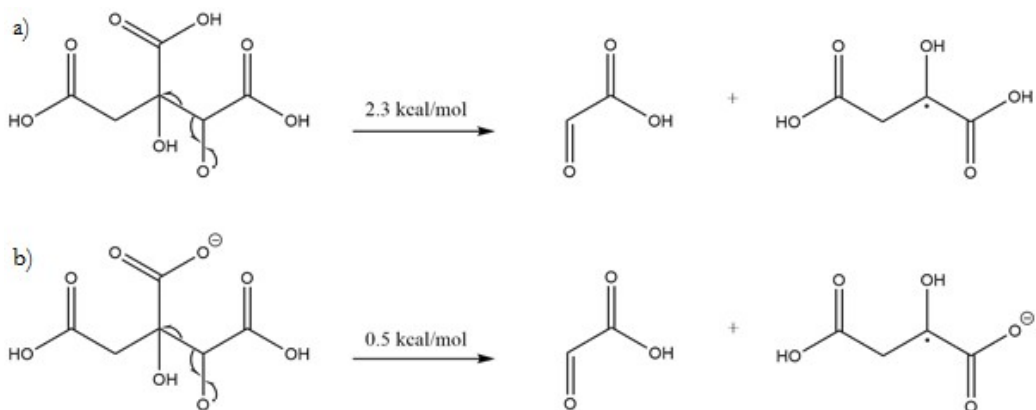


891

892

893

## Scheme 2



894

895

896

897

898

899

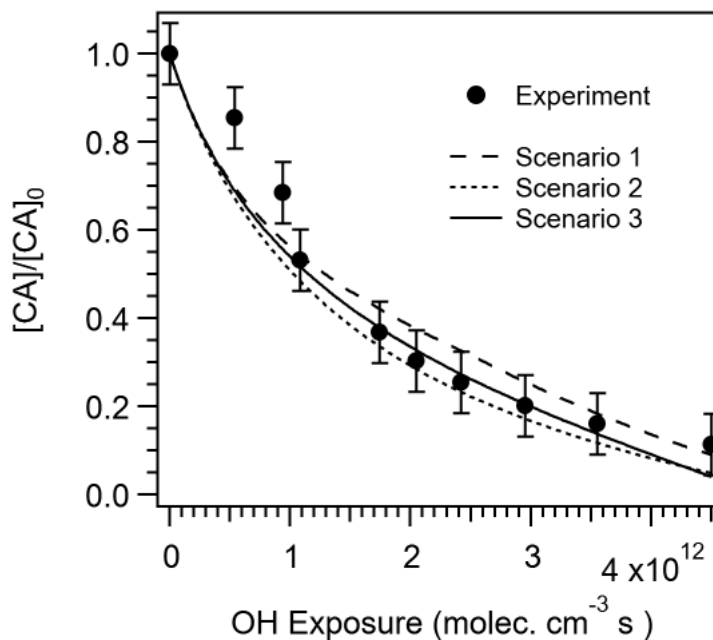
75

76

900

901

902



903

904 **Figure 2.** Experimental and simulated reactive decay of CA as a function of OH exposure. The  
905 experimental and simulation results were normalized to unreacted  $[CA]_0$  prior to heterogeneous  
906 reaction. See Table 1 for simulation parameters and Table 2 for scenario descriptions.

907

908

909

910

911

912

913

914

915

916

917

918

77

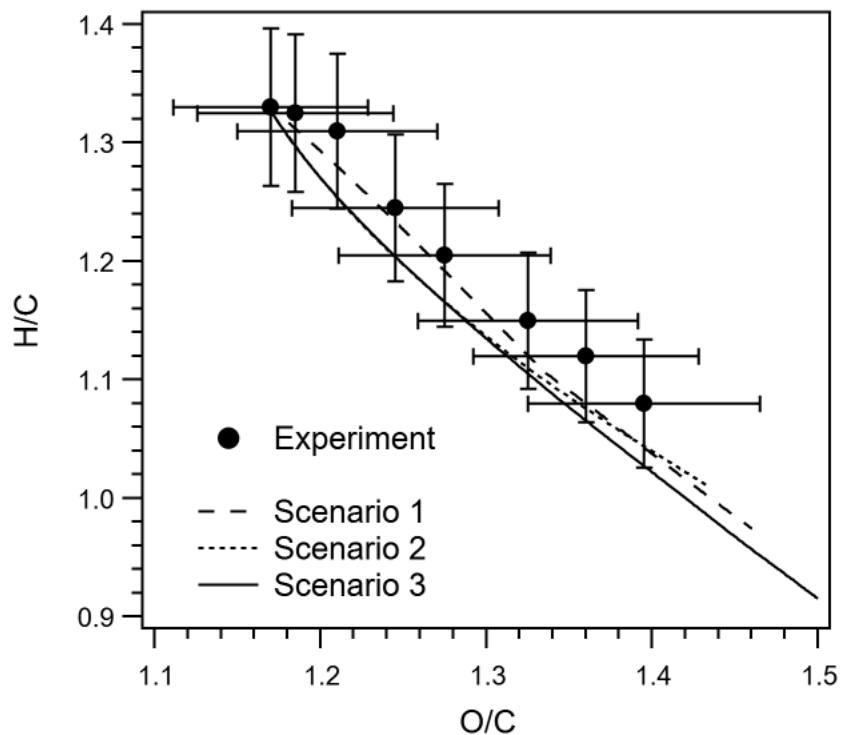
78



919

920

921



922

923 **Figure 3.** Experimental and simulated Van Krevelen plots (H/C vs. O/C) of average aerosol  
924 elemental composition. Simulation results fall within experimental error regardless of the model  
925 scenario. Note unreactive CA has H/C = 1.33 and O/C = 1.16. As the reaction progress the  
926 average H/C of the aerosol decreases and the O/C increases.

927

928

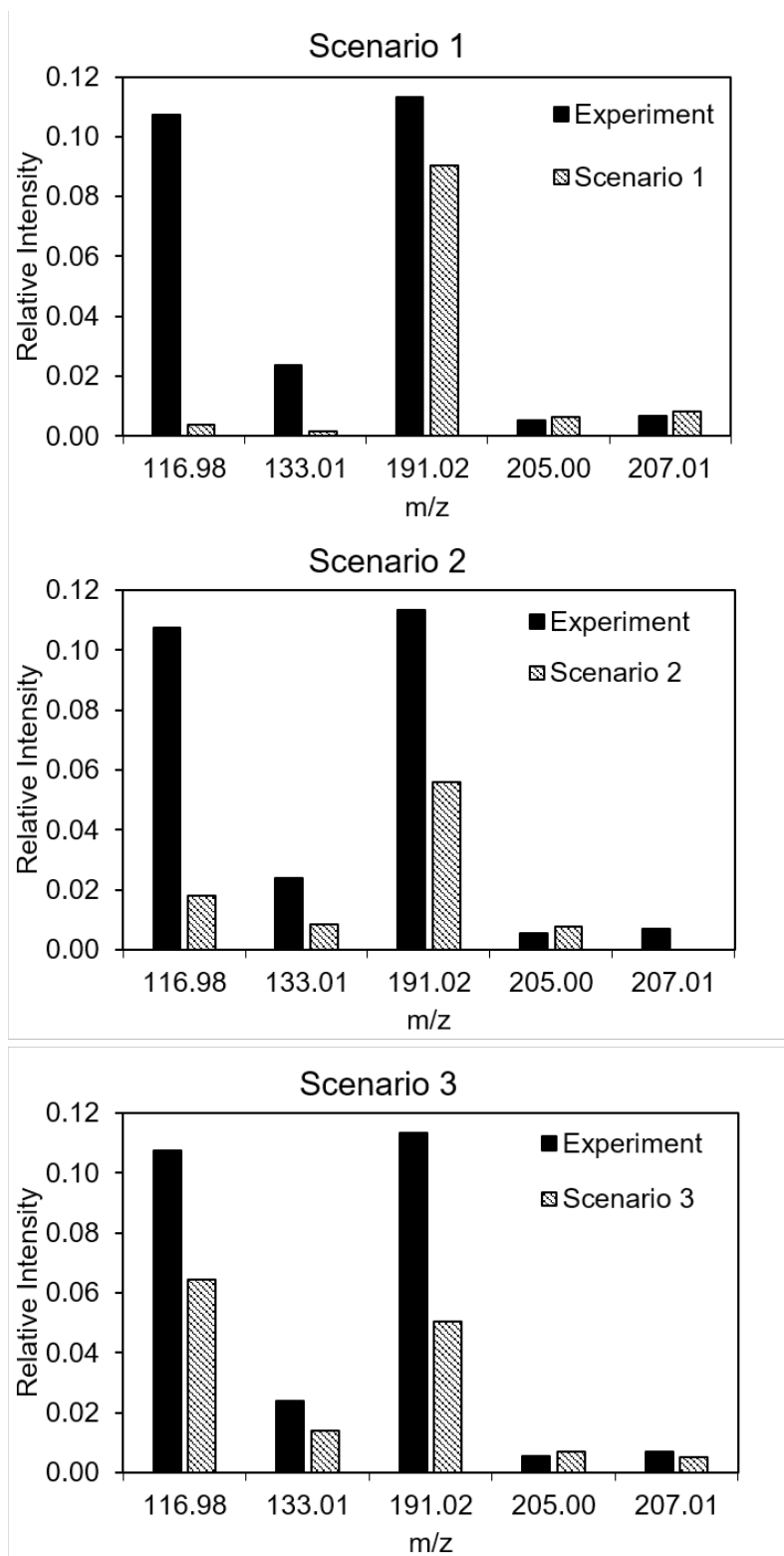
929

930

931

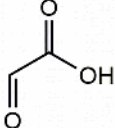
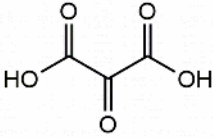
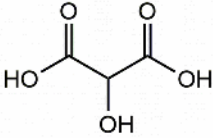
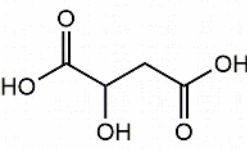
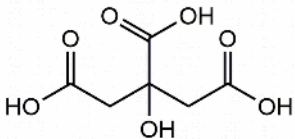
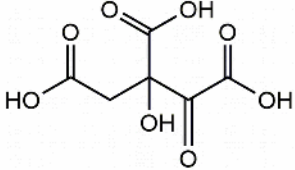
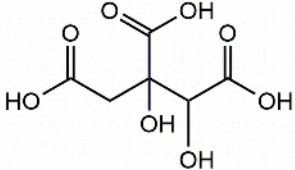
932

933



934

935 **Figure 4.** Experimental and simulated negative ion mass spectra of the major oxidation products  
 936 of CA produced at an OH exposure of  $4.4 \times 10^{12}$  molecules  $\text{s cm}^{-3}$ . See Figure 5 for structures of  
 937 these reaction products.

m/z	-ve ion	Structure	pKa	O/C	H/C
73.03	C <sub>2</sub> HO <sub>3</sub>		3.32	1.50	1.00
116.98	C <sub>3</sub> HO <sub>5</sub>	 Mesoxalic acid	1.15	1.67	0.67
119.00	C <sub>3</sub> H <sub>3</sub> O <sub>5</sub>		1.98	1.67	1.33
133.01	C <sub>4</sub> H <sub>5</sub> O <sub>5</sub>	 Malic Acid	3.40	1.25	1.50
191.02	C <sub>6</sub> H <sub>7</sub> O <sub>7</sub>	 Citric Acid	3.13	1.17	1.33
205.00	C <sub>6</sub> H <sub>5</sub> O <sub>8</sub>		2.23	1.33	1.00
207.01	C <sub>6</sub> H <sub>7</sub> O <sub>8</sub>		2.90	1.33	1.33

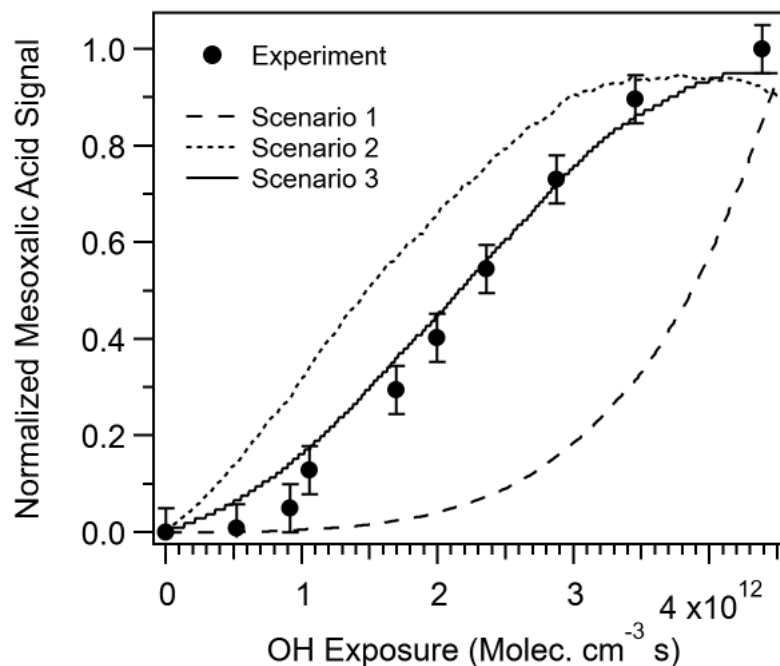
938

939 **Figure 5:** Molecular structures, negative ion m/z, H/C, O/C and pK<sub>a</sub> of the major reaction  
940 products observed experimentally by Davies and Wilson.<sup>37</sup>

941

942

943  
944  
945  
946



947

948 **Figure 6:** Experimental and simulated concentration of mesoxalic acid ( $m/z = 116.98$ ) as  
949 function of OH exposure. For comparison the experimental and simulated concentration was  
950 normalized to the maximum value. Scenario 3 predictions are within experimental error.

951

952

953

954

955

956

957

958

959

960

961

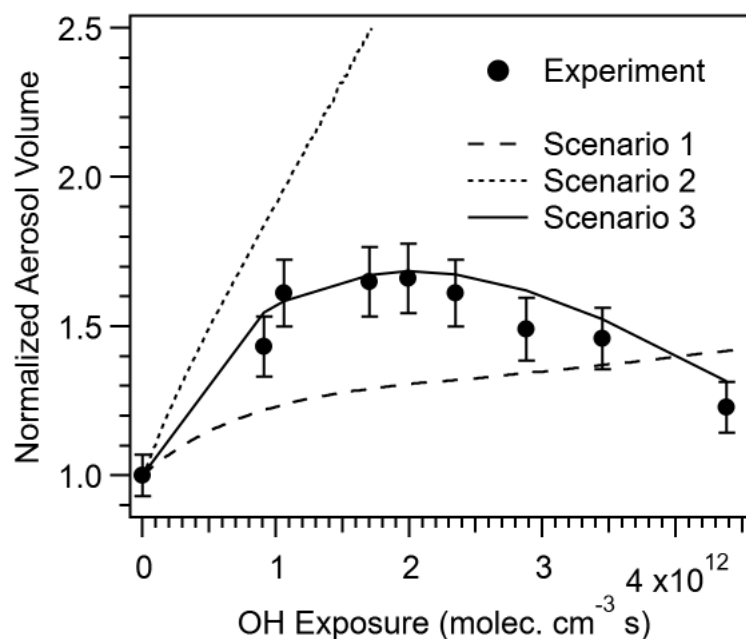
85

86

962

963

964



965

966**Figure 7:** Experimental and simulated normalized aerosol volume as a function of OH exposure.  
967The volume is normalized to the unreacted CA aerosol. The rapid growth observed in Scenario 2  
968is due to lack of evaporation in this scenario. Scenario 1 fails to capture the initial increase in  
969volume and similar to scenario 1, does not predict the decrease in volume due to a lack of  
970evaporation. Scenario 3 is the only model to predict within experimental error the complex  
971growth and decay in aerosol volume observed over the course of the reaction.

972

973

974

975

976

977

978

979

980

981

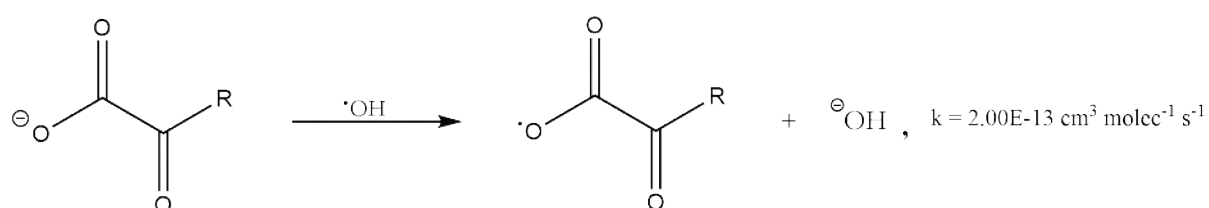
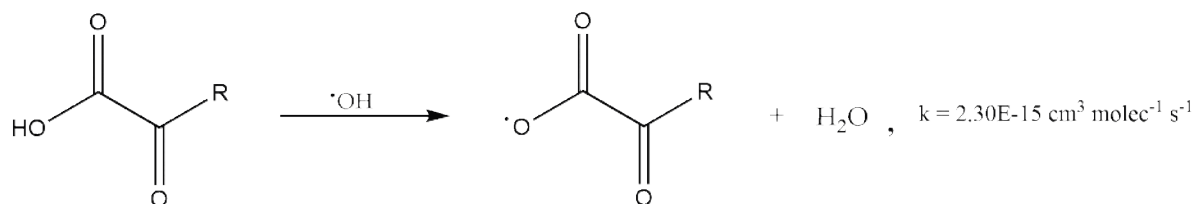
87

88

982

983

984



985

986**Figure 8:** A comparison in acyloxy radical formation rate between an  $\alpha$ -keto acid and its  
987conjugate base. The charge transfer reaction of the base (bottom) has a rate coefficient that is  
988approximately 2 orders of magnitude larger than the hydrogen abstraction reaction on the acid  
989(top). The inclusion of acid-base chemistry substantially increases acyloxy radical formation  
990rates.

991

992

993

994

995

996

997

998

999

1000

1001

1002

1003

89

90

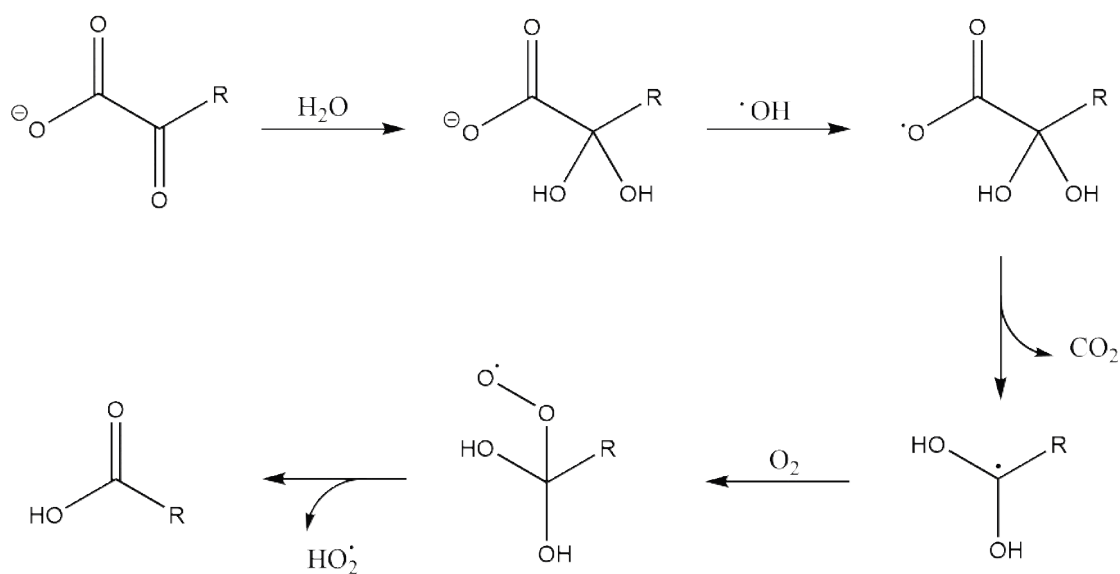
1004

1005

1006

1007

1008



1009

1010**Figure 9:** Carboxyl group formation accompanied by one-carbon loss via acyloxy radical  
 1011formation. After decarboxylation of the acyloxy radical, addition of oxygen to the resulting  
 1012alpha-di-hydroxyalkyl radical and subsequent decomposition yields an acid that differs only by 1  
 1013carbon atom from the original reactant. Hydration is an essential part of this pathway, making it  
 1014unique to the aqueous-phase.

1015

1016

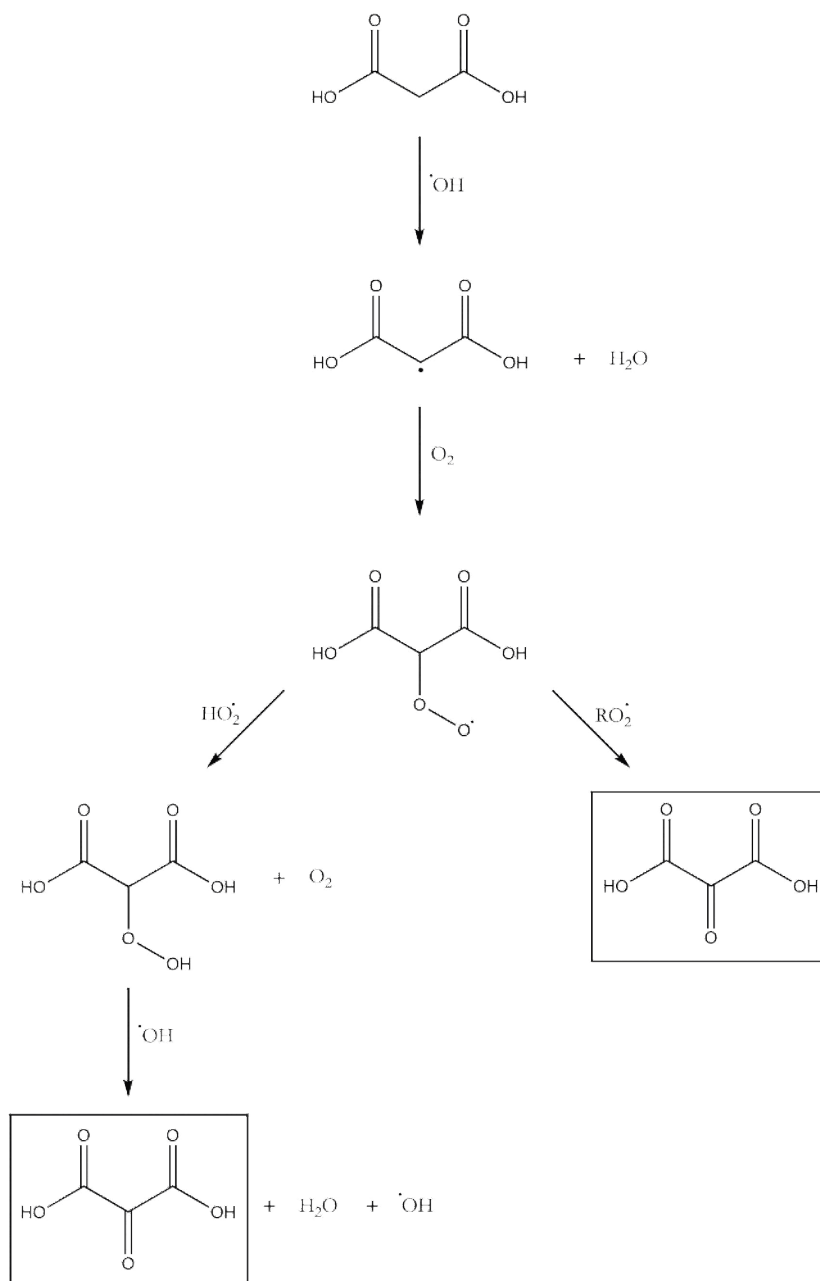
1017

1018

1019

1020

1021



1022

1023 **Figure 10:** The two reaction pathways that produce mesoxalic acid ( $m/z = 116.98$ ). In the right  
 1024 branch,  $\text{RO}_2$  may also react to yield 2-hydroxymalonic acid (i.e.  $\text{C}_3\text{H}_4\text{O}_5$ , tartronic acid). The  
 1025  $\text{ROOH} + \text{OH}$  reaction in the left branch regenerates  $\text{OH}$  further propagating the reaction.

1026

1027

1028

1029

1030

1031

1032

1033

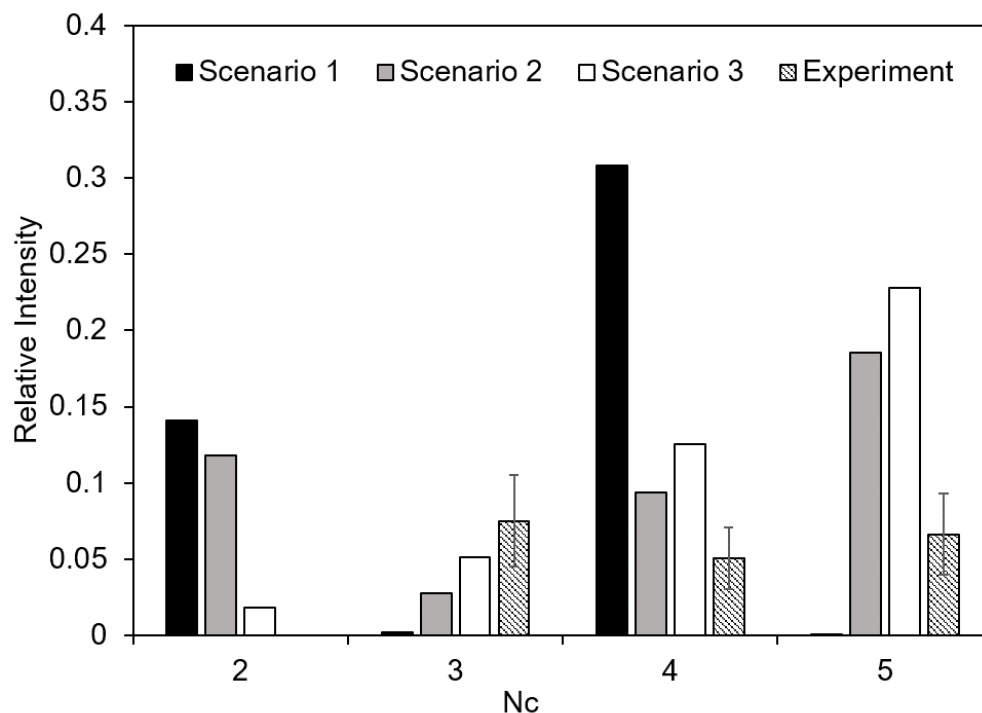
93

47

94



1034  
1035  
1036  
1037  
1038



1039

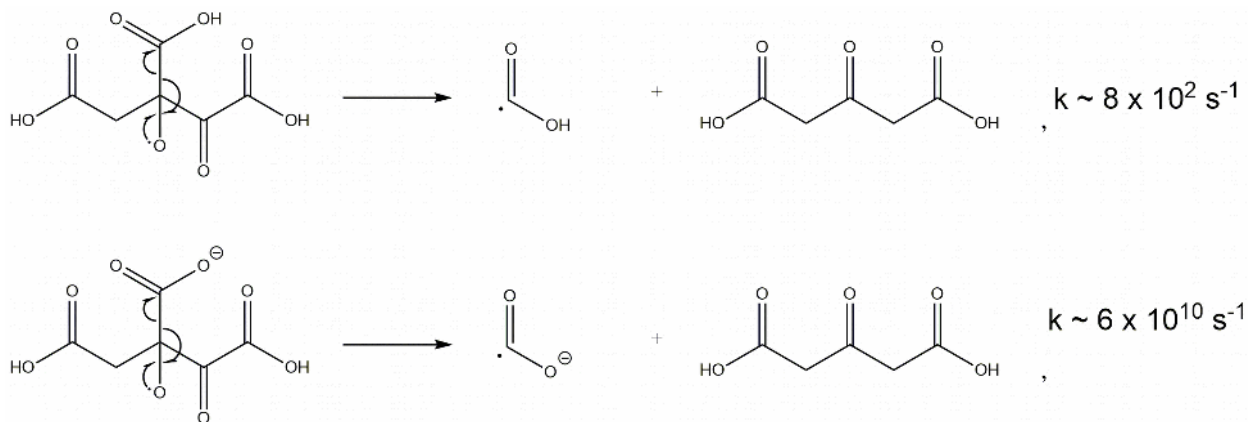
1040 **Figure 11:** Simulated product carbon number ( $N_c$ ) distributions (at OH exposure =  $2.2 \times 10^{12}$   
1041  $\text{molec. cm}^{-3} \text{ s}$ ) for Scenarios 1, 2 and 3. The experimental data are also shown at OH exposure =  
1042  $2.1 \times 10^{12} \text{ molec. cm}^{-3} \text{ s}$ , for qualitative comparison to the calculations. Each carbon number is  
1043 computed by dividing the sum of all species corresponding to a carbon number by the initial  
1044 concentration of CA. Scenario 1 lacks  $C_5$  products, which are only produced when acid-base  
1045 chemistry is included in the reaction scheme (i.e. Scenario 2 and 3).

1046

1047  
1048  
1049  
1050  
1051  
1052  
1053  
1054  
1055  
1056  
1057  
1058

95  
96

1059  
1060  
1061  
1062  
1063  
1064  
1065  
1066

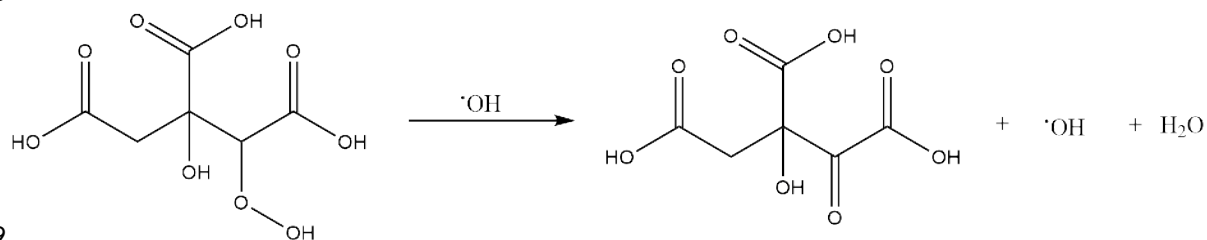


1067

1068**Figure 12:** Computed rate coefficients for the unimolecular decomposition of alkoxy radicals  
1069(see text for details). Fragmentation of the radical anion (bottom) is many orders of magnitude  
1070faster than the neutral case (top).

1071  
1072  
1073  
1074  
1075  
1076  
1077  
1078  
1079  
1080  
1081  
1082  
1083  
1084  
1085  
1086  
1087  
1088  
1089  
1090  
1091  
1092  
1093  
1094  
1095  
1096  
1097  
1098

1099  
1100  
1101  
1102  
1103  
1104  
1105  
1106  
1107  
1108



1109

1110 **Figure 13:** A significant reaction pathway that converts a ROOH group into a carbonyl with  $\text{H}_2\text{O}$   
1111 and  $\text{OH}$  as coproducts.

1112  
1113

1114

1115

1116

1117

1118

1119

1120TOC Graphic

1121

1122

1123

1124

1125

